Computational homogenization

M.G.D. Geers [*], V.G. Kouznetsova [*†], W.A.M. Brekelmans [*]
[*] Eindhoven University of Technology
Department of Mechanical Engineering Eindhoven
[†] Netherlands Institute for Metals Research

Abstract This part of the CISM course addresses basics and advanced topics on the computational homogenization of the mechanics of highly non-linear solids with (possibly evolving) microstructure under complex non-linear loading conditions. The key components of the computational homogenization scheme, i.e. the formulation of the microstructural boundary value problem and the coupling between the micro and macrolevel based on the averaging theorems, are addressed. The numerical implementation of the framework, particularly the computation of the macroscopic stress tensor and extraction of the macroscopic consistent tangent operator based on the total microstructural stiffness, are treated in detail. The application of the method is illustrated by the simulation of pure bending of porous aluminum. The classical notion of a representative volume element is introduced and the influence of the spatial distribution of heterogeneities on the overall macroscopic behaviour is investigated by comparing the results of multi-scale modelling for regular and random structures. Finally, an extension of the classical computational homogenization scheme to a framework suitable for multi-scale modelling of macroscopic localization and size effects is briefly discussed.

1 Introduction

The past years have been marked by a significant interest in the various length scales that govern the mechanics of materials. The main issue consists in identifying the relationships that bridge those various scales, i.e. multi-scale mechanics. The multi-scale methodology aims to predict, describe, quantify or qualify the 'macroscopic' behaviour of engineering materials through the consistent modelling of the mechanics and physics of the heterogeneous, multi-phase, anisotropic, discrete microstructure. Various techniques have been proposed to contribute to this challenging task. Among them, a large class of homogenization techniques exists, also called

coarse graining in the physics community (Ridderbos, 2002; Nguyen and Ortiz, 2002).

Homogenization techniques were first developed within the framework of elasticity, as an excellent tool to predict the effective or apparent linear elastic properties of heterogeneous materials. Several closed-form homogenization techniques have been proposed in this context, e.g. the Voigt-Reuss-Hill bounds, the Hashin-Shtrikman variational principle, the self-consistent method, etc., see (Nemat-Nasser and Hori, 1993) for an overview. Asymptotic or mathematical homogenization schemes have been used frequently to assess effective properties of elastic heterogeneous materials (Chung et al., 2001; Fish and Chen, 2001). Extensions towards higher-order and nonlocal constitutive equations have been considered as well, e.g. developments including Cosserat media (Forest et al., 2001), couple stress theory (Smyshlyaev and Fleck, 1994), nonlocal effective continua (Drugan and Willis, 1996) or higher-order gradient homogenized elastic materials (Triantafyllidis and Bardenhagen, 1996; Smyshlyaev and Cherednichenko, 2000; Peerlings and Fleck, 2001).

Other interesting approaches towards the analysis of random (physically nonlinear) microstructures (Ponte Castañeda, 1992; Suquet, 1993; Ponte Castañeda, 2002) are the Taylor-Bishop-Hill estimates, several generalizations of self-consistent schemes and asymptotic procedures (Fish et al., 1997). Homogenization of solids in a geometrically and physically nonlinear regime is clearly more cumbersome. Several analyses have been performed on unit cells, from which the parameters in a priori assumed macroscopic constitutive equations can be assessed. Some of them also include higher-order continuum formulations, e.g. Cosserat (van der Sluis et al., 1999) and couple stress media (M. Ostoja-Starzewski, 1999). The added value of these multi-scale methods depends on the accuracy (geometrical, physical, mechanical) with which the microstructure is modelled, as well as the technique that is used to perform the homogenization towards the macroscopic level. Closed-form homogenization towards constitutive material frameworks or effective (or rather apparent) material properties of composites turns out to be really cumbersome if one wishes to take into account more complex physics, geometrical nonlinearities or damage and localization.

Another class of hierarchical techniques are generally known as variational multi-scale methods (Hughes et al., 1998; Garikipati and Hughes, 2000). In here, the weak form of the governing equations is the point of departure, which can be separated in a coarse and a fine scale part on the basis of suitable assumptions on the fine scale field. The key issue resides in the elimination of the fine scale from the obtained formulation. Though promising, the method relies strongly on the assumptions made on

the fine scale and the restrictions that apply to enable the elimination in practice. Well-known fine scale patterns, e.g. displacement discontinuities modelled by Heaviside functions, can be easily implemented. The obtained method then shows considerable similarities with the extended finite element method (Sukumar et al., 2000; Moës and Belytschko, 2002).

Since a few years, substantial progress has been made in the two-scale computational homogenization of complex multi-phase solids. This technique is essentially based on the solution of nested boundary value problems, one for each scale. If attention is focused on the nonlinear characteristics of the material behaviour, this technique proves to be a valuable tool in retrieving the constitutive response. First-order (i.e. including first-order gradients of the macroscopic displacement field only) computational homogenization schemes fit entirely in a standard continuum mechanics framework (principle of local action) and are now readily available in literature (Suquet, 1985; Ghosh et al., 1996; Smit et al., 1998; Miehe et al., 1999b,a; Feyel and Chaboche, 2000; Terada et al., 2000; Ghosh et al., 2001; Kouznetsova et al., 2001; Terada and Kikuchi, 2001; Miehe and Koch, 2002). Main characteristics of this solution strategy are

- The constitutive response at the macro scale is a priori undetermined. No explicit assumptions are required at that level, since the macroscopic constitutive behaviour ensues from the solution of the micro scale boundary value problem.
- The method deals with large displacements (large strains and rotations) in a trivial way under the condition that the microstructural constituents are modelled adequately.
- The different phases in the microstructure can be modelled with arbitrary nonlinear and time-dependent constitutive models.
- The influence of the evolution of the microstructure (as described on the micro-scale) can be assessed directly on the macro-scale.
- The micro scale problem is a classical boundary value problem, for which any appropriate solution strategy can be used, e.g. Finite Element Method (Smit et al., 1998; Feyel and Chaboche, 2000; Terada et al., 2000; Kouznetsova et al., 2001), the Voronoi cell method (Ghosh et al., 1995, 1996), a crystal plasticity framework (Miehe et al., 1999b,a) or numerical methods based on Fast Fourier Transforms (Michel et al., 1999; Moulinec and Suquet, 1998). Galerkin, etc.
- Macroscopic constitutive tangent operators can be obtained from the microscopic overall stiffness tensor through static condensation. Consistency is preserved through this scale transition.

In spite of the huge computational cost of a nested two-scale solution problem, efficiency can be achieved by solving the problem through parallel

computations (Feyel and Chaboche (2000); Kouznetsova (2002)). Another option is selective usage, where non-critical regions are modelled by continuum closed-form homogenized constitutive relations or by the constitutive tangents obtained from the microstructural analysis but kept constant in the elastic domain, while in the critical regions the multi-scale analysis of the microstructure is fully performed (Ghosh et al. (2001)). Despite the required computational efforts the computational homogenization technique has proven to be a valuable tool to establish non-linear micro-macro structure-property relations, especially in the cases where the complexity of the mechanical and geometrical microstructural properties and the evolving character prohibit the use of other homogenization methods.

Cartesian tensors and associated tensor products will be used throughout this chapter, making use of a Cartesian vector basis $\{\vec{e}_1, \vec{e}_2, \vec{e}_3\}$. Using the Einstein summation rule for repeated indices, the following conventions are used in the notations of well-known tensor products

$$\begin{aligned}
\mathbf{C} &= \vec{a}\,\vec{b} = a_i b_j \,\vec{e}_i\,\vec{e}_j \\
\mathbf{C} &= \mathbf{A}\cdot\mathbf{B} = A_{ij}B_{jk}\,\vec{e}_i\,\vec{e}_k \\
\mathbf{C} &= {}^4\mathbf{A} : \mathbf{B} = A_{ijkl}B_{lk}\,\vec{e}_i\,\vec{e}_j \\
\mathbf{C} &= {}^4\mathbf{A} \vdots {}^4\mathbf{B} = A_{iklm}B_{mlkj}\,\vec{e}_i\,\vec{e}_j
\end{aligned}$$

2 Underlying principles and assumptions

2.1 Scale separation

At the macro-scale, the material is considered as a homogeneous continuum, whereas at the micro level it is generally heterogeneous (the morphology consists of distinguishable components or phases, i.e. inclusions, grains, interfaces, cavities, etc.). This is schematically illustrated in figure 1. The microscopic length scale is much larger than the molecular dimensions

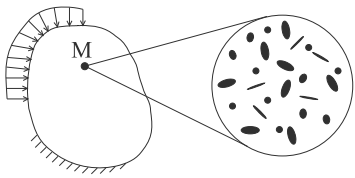

Figure 1. Macroscopic continuum point representation (M) in relation to its underlying heterogeneous microstructure.

$\ell_{discrete}$, so that a continuum approach is justified for every constituent. At the same time, in the context of the *principle of separation of scales*, the microscopic length scale ℓ_{micro} is assumed to be much smaller than the characteristic length ℓ_{macro} over which the size of the macroscopic loading varies in space, i.e.

$$\ell_{discrete} \lll \ell_{micro} \lll \ell_{macro} \tag{1}$$

Note that it is not the size of the macroscopic domain which is important, but rather the spatial variation of the kinematic fields and stress fields within that domain.

2.2 Local periodicity

Most of the homogenization approaches rely on the assumption of *global periodicity* of the microstructure, implying that the whole macroscopic domain consists of spatially repeated unit cells. In a computational homogenization approach, a more realistic assumption is made, which is commonly denoted by *local periodicity*. According to this assumption, the microstructure can have different morphologies corresponding to different macroscopic points, whereas it repeats itself only in a small vicinity of each individual macroscopic point. The concepts of local and global periodicity are schematically illustrated in figure 2. The assumption of local periodicity adopted in the computational homogenization allows to incorporate a non-uniform distribution of the microstructure at the macroscopic level (e.g. in functionally graded materials). Note that the local periodicity assumption is directly linked to the principle of separation of scales.

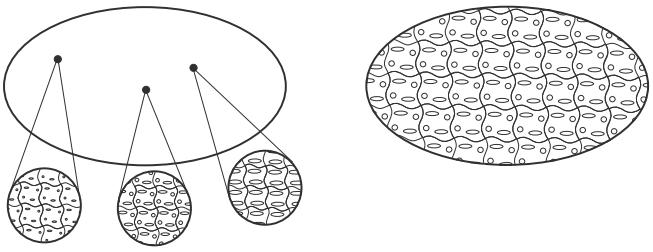

(a) local periodicity (b) global periodicity

Figure 2. Local periodicity (a) versus global periodicity (b).

2.3 Homogenization principles

The basic principles of computational homogenization have gradually evolved from the concepts employed in other homogenization methods and well fit into the four-step homogenization scheme established by Suquet Suquet (1985):

1. definition of a microstructural representative volume element (RVE), of which the constitutive behaviour of individual constituents is assumed to be known;
2. formulation of the microscopic boundary conditions from the macroscopic input variables and their application on the RVE (macro-to-micro transition);
3. calculation of the macroscopic output variables from the analysis of the deformed microstructural RVE (micro-to-macro transition);
4. obtaining the (numerical) relation between the macroscopic input and output variables.

The main ideas of the first-order computational homogenization have been established in Suquet (1985); Guedes and Kikuchi. (1990); Terada and Kikuchi (1995); Ghosh et al. (1995, 1996) and further developed and improved in more recent works Smit et al. (1998); Miehe et al. (1999b); Miehe and Koch (2002); Michel et al. (1999); Feyel and Chaboche (2000); Terada and Kikuchi (2001); Ghosh et al. (2001); Kouznetsova et al. (2001); Kouznetsova (2002).

2.4 Computational homogenization scheme

A computational homogenization generally departs from the computation of a macroscopic deformation (gradient) tensor $\mathbf{F}_{\mathrm{M}}$, which is calculated for every material point of the macrostructure (e.g. the integration points within a macroscopic finite element domain). Here and in the following the subscript "M" refers to a macroscopic quantity, while the subscript "m" will denote a microscopic quantity. The deformation tensor $\mathbf{F}_{\mathrm{M}}$ for a macroscopic point is next used to formulate the boundary conditions to be imposed on the RVE that is assigned to this point. Upon the solution of the boundary value problem for the RVE, the macroscopic stress tensor $\mathbf{P}_{\mathrm{M}}$ is obtained by averaging the resulting RVE stress field over the volume of the RVE. As a result, the (numerical) stress-deformation relationship at the macroscopic point is readily available. Additionally, the local macroscopic consistent tangent is extracted from the microstructural stiffness. The entire framework is schematically illustrated in figure 3. The computational homogenization technique defined in this sense, is entirely consistent with the principle of local action in continuum mechanics. Therefore, the response at

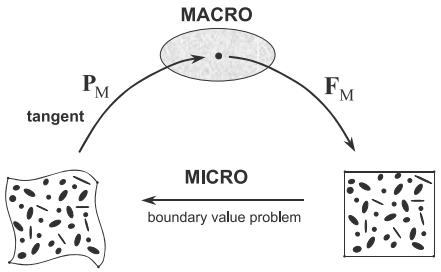

Figure 3. Computational homogenization scheme.

a (macroscopic) material point depends only on the first gradient of the displacement field. This macroscopically local computational homogenization framework may therefore be categorized as a "first-order" approach.

2.5 Kinematically driven multi-scale scheme

The multi-scale procedure outlined in this chapter is "deformation driven". The point of departure is thereby the macroscopic deformation gradient tensor $\mathbf{F}_M$, which is used to determine the stress $\mathbf{P}_M$ and the constitutive tangent, based on the response of the underlying microstructure. A "stress driven" procedure (given a local macroscopic stress, obtain the deformation) is also possible. However, such a procedure does not directly fit into a standard displacement-based finite element framework, which will be here employed to solve the macroscopic boundary value problem. Moreover, in case of large deformations the macroscopic rotational effects have to be added to the stress tensor in order to uniquely determine the deformation gradient tensor, thus complicating the implementation. Therefore, the "stress driven" approach, which is often used in the analysis of single unit cells, is generally not adopted in coupled multi-scale computational homogenization strategies of the type described here.

3 The micro-scale problem

3.1 The representative volume element

The physical and geometrical properties of the microstructure are identified by a representative volume element (RVE) (Hill, 1963; Drugan and Willis, 1996). An example of a typical two-dimensional RVE is depicted in figure 4. The actual choice of the RVE is a rather delicate task. The RVE should be large enough to represent the microstructure, without introducing

non-existing properties (e.g. undesired anisotropy) and at the same time it should be small enough to allow efficient computational modelling. Some issues related to the concept of a representative cell are discussed furtheron, in section 7. Here it is supposed that an appropriate RVE has been already selected. Then the problem on the RVE level can be formulated as a standard problem in quasi-static continuum solid mechanics.

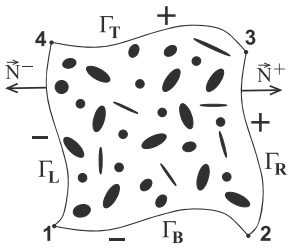

Figure 4. Schematic picture of a typical two-dimensional representative volume element (RVE).

3.2 Micro-scale characterization & equilibrium

The RVE deformation field in a point with the initial position vector $\vec{X}$ (in the reference domain V_0) and the actual position vector $\vec{x}$ (in the current domain V) is described by the microstructural deformation gradient tensor $Fm = (\vec{\nabla}_{0,\mathrm{m}}\vec{x})^c$, where the gradient operator $\vec{\nabla}_{0,\mathrm{m}}$ is taken with respect to the reference microstructural configuration; the superscript "c" indicates conjugation.

The RVE is in a state of equilibrium. This is mathematically expressed through the standard equilibrium equation in terms of the Cauchy stress tensor $\boldsymbol{\sigma}_\mathrm{m}$ or, alternatively, in terms of the first Piola-Kirchhoff stress tensor $\mathbf{P}_\mathrm{m} = \det(\mathbf{F}_\mathrm{m})\boldsymbol{\sigma}_\mathrm{m}{\cdot}(\mathbf{F}_\mathrm{m}^c)^{-1}$ according to (in the absence of body forces)

$$\vec{\nabla}_\mathrm{m}{\cdot}\boldsymbol{\sigma}_\mathrm{m} = \vec{0} \quad \text{in} \quad V, \qquad \text{or} \qquad \vec{\nabla}_{0,\mathrm{m}}{\cdot}\mathbf{P}_\mathrm{m}^c = \vec{0} \quad \text{in} \quad V_0, \tag{2}$$

where $\vec{\nabla}_\mathrm{m}$ is the the gradient operator with respect to the current configuration at the micro-scale.

The mechanical characterization of the microstructural components are described by their constitutive laws, specifying a time and history dependent stress-deformation relationship for every microstructural constituent

$$\boldsymbol{\sigma}_\mathrm{m}^{(\alpha)}(t) = \boldsymbol{\mathcal{F}}_\sigma^{(\alpha)}\{\mathbf{F}_\mathrm{m}^{(\alpha)}(\tau),\ \tau \in [0,t]\}, \ \text{ or } \ \mathbf{P}_\mathrm{m}^{(\alpha)}(t) = \boldsymbol{\mathcal{F}}_P^{(\alpha)}\{\mathbf{F}_\mathrm{m}^{(\alpha)}(\tau),\ \tau \in [0,t]\}, \tag{3}$$

where t denotes the current time; $\alpha = \overline{1, N}$, with N the number of microstructural constituents to be distinguished (e.g. matrix, inclusions, etc.). Note that the knowledge of the separate constitutive laws for each of the individual phases is essential.

3.3 The macro-micro scale transition

The macro-micro scale transition requires a method to impose the macroscopic deformation gradient tensor $\mathbf{F}_{\mathrm{M}}$ or stress tensor $\mathbf{P}_{\mathrm{M}}$ on the microstructural RVE. Classical simplified methods to do this are:

- by imposing that all the microstructural constituents undergo a constant deformation identical to the macroscopic one (the Taylor or Voigt assumption).
- by imposing an identical constant stress (and additionally identical rotation) to all the components (the Sachs or Reuss) assumption).
- by intermediate procedures, where the Taylor and Sachs assumptions are applied only to certain components of the deformation and stress tensors.

These simplified procedures do not satisfy all local static equilibrium and compatibility conditions and generally provide only rough estimates of the overall material properties. They are therefore not well-suited in complex non-linear deformation regimes. The Taylor assumption usually overestimates the overall stiffness, while the Sachs assumption leads to an underestimation of the stiffness. A computational homogenization scheme does enforce local equilibrium and compatibility between phases, and therefore necessitates a different macro-micro scale transition method.

The first-order scheme naturally departs from the classical linearization of the macroscopic nonlinear deformation map, $\vec{x} = \phi(\vec{X})$, applied to a finite material vector $\Delta\vec{x}$ in the deformed state:

$$\Delta\vec{x} \;=\; \mathbf{F}_{\mathrm{M}}{\cdot}\Delta\vec{X} + \mathcal{O}\left(\Delta\vec{X}^2\right), \tag{4}$$

with $\vec{x}$ and $\vec{X}$ associated position vectors in the deformed and reference state, respectively, and in which $\mathbf{F}_{\mathrm{M}} = (\vec{\nabla}_{0,\mathrm{M}}\vec{x})^T$ is the macroscopic deformation gradient tensor. Considering an undeformed volume V_0 of material with its centre positioned at $\vec{X}_c$, permits to write the deformed position of any point of this volume (with respect to the centre of that volume) as the sum of a macroscopic (or coarse scale) and a microscopic (or fine scale) contribution:

$$\vec{x} - \vec{x}_c \;=\; \mathbf{F}_{\mathrm{M}}{\cdot}(\vec{X} - \vec{X}_c) + \vec{w} \tag{5}$$

The fine scale contribution is here represented by the microfluctuation field $\vec{w}$. The vector $\vec{x}_c$ is the actual position of the reference RVE center $\vec{X}_c$.

Obviously, rigid body displacements have to be eliminated to uniquely determine $\vec{x}$. An arbitrary boundary point may be fixed to this purpose, e.g. for a point with label 1 (see figure 4) by imposing $\vec{x}_1 = \vec{X}_1$. Substituting this in (5) leads to

$$\vec{x} \;=\; \vec{c} + \mathbf{F}_{\mathrm{M}} \cdot (\vec{X} - \vec{X}_c) + (\vec{w} - \vec{w}_1) \tag{6}$$

where $\vec{w}_1$ is the microfluctuation in point 1 and where vector $\vec{c}$ is determined from $\vec{X}_1$, being independent of the fine scale field

$$\vec{c} \;=\; \vec{X}_1 - \mathbf{F}_{\mathrm{M}} \cdot (\vec{X}_1 - \vec{X}_c) \tag{7}$$

The deformed position $\vec{x}_c$ of the reference centre $\vec{X}_c$ is then (using the trivial relation $\vec{w}_c = \vec{0}$) given by

$$\vec{x}_c \;=\; \vec{c} - \vec{w}_1 \tag{8}$$

Note that this deformed position is unknown and implicitly depends on the fine scale field. The scale transition between the kinematics at the fine and the coarse scale typically involves the volume average $\bar{\mathbf{F}}_{\mathrm{m}}$ of the fine scale deformations tensors, i.e.

$$\bar{\mathbf{F}}_{\mathrm{m}} \;=\; \frac{1}{V_0} \int_{V_0} \mathbf{F}_{\mathrm{m}} dV_0 \tag{9}$$

This volume integral can be rewritten to the boundary Γ_0 of the RVE by making use of the divergence theorem

$$\begin{aligned} \bar{\mathbf{F}}_{\mathrm{m}} \;&=\; \frac{1}{V_0} \int_{V_0} \mathbf{F}_{\mathrm{m}} dV_0 \;=\; \frac{1}{V_0} \int_{V_0} \left(\vec{\nabla}_{0,\mathrm{m}} \cdot (\mathbf{I}\vec{x}) \right)^c dV_0 \\ &=\; \frac{1}{V_0} \int_{\Gamma_0} \left(\vec{N} \cdot (\mathbf{I}\vec{x}) \right)^c d\Gamma_0 \\ &=\; \frac{1}{V_0} \int_{\Gamma_0} \vec{x}\vec{N} d\Gamma_0 \end{aligned} \tag{10}$$

where $\mathbf{I}$ represents the second-order unit tensor, Γ_0 the external boundary of the undeformed RVE V_0 and $\vec{N}$ the outward unit normal on that boundary.

Computing the fine scale deformation gradient tensor $\mathbf{F}_{\mathrm{m}}$ by taking the fine scale spatial gradient of the position vector given in equation (6) results in

$$\mathbf{F}_{\mathrm{m}} = (\vec{\nabla}_{0,\mathrm{m}} \vec{x})^c \;=\; \mathbf{F}_{\mathrm{M}} + (\vec{\nabla}_{0,\mathrm{m}} (\vec{w} - \vec{w}_1))^c \;=\; \mathbf{F}_{\mathrm{M}} + (\vec{\nabla}_{0,\mathrm{m}} \vec{w})^c \tag{11}$$

Alternatively, making use of the micro-fluctuation field, $\bar{\mathbf{F}}_{\mathrm{m}}$ can be expanded to

$$\begin{aligned}\bar{\mathbf{F}}_{\mathrm{m}} &= \mathbf{F}_{\mathrm{M}} + \frac{1}{V_0}\int_{V_0}[\vec{\nabla}_{0,\mathrm{m}}(\vec{w}-\vec{w}_1)]^c \mathrm{d}V_0 = \mathbf{F}_{\mathrm{M}} + \frac{1}{V_0}\int_{V_0}[\vec{\nabla}_{0,\mathrm{m}}\vec{w}]^c \mathrm{d}V_0 \\ &= \mathbf{F}_{\mathrm{M}} + \frac{1}{\Gamma_0}\int_{\Gamma_0}(\vec{w}-\vec{w}_1)\vec{N}\mathrm{d}\Gamma_0 = \mathbf{F}_{\mathrm{M}} + \frac{1}{\Gamma_0}\int_{\Gamma_0}\vec{w}\vec{N}\mathrm{d}\Gamma_0\end{aligned} \tag{12}$$

In the case where $\mathbf{F}_{\mathrm{M}}$ is known and displacements at the RVE boundary are to be prescribed are constrained, use is made of a scale transition relation that enforces the macroscopic deformation gradient $\mathbf{F}_{\mathrm{M}}$ to equal the volume average of its microscopic counterparts $\bar{\mathbf{F}}_{\mathrm{m}}$,

$$\mathbf{F}_{\mathrm{M}} = \bar{\mathbf{F}}_{\mathrm{m}} \tag{13}$$

Enforcing the scale transition relation (13) clearly leads to a constraint in the form of a boundary integral

$$\int_{\Gamma_0}(\vec{w}-\vec{w}_1)\vec{N}d\Gamma_0 = \mathbf{0} = \int_{\Gamma_0}\vec{w}\vec{N}d\Gamma_0 \tag{14}$$

The boundary integral (14) is the necessary condition that enforces the averaging theorem (13), which will be used in the scale transition, see also (Miehe et al., 2002). Stronger conditions are obtained by making specific choices for $\vec{w}$ that enforce this boundary integral to vanish. A few possible choices for these boundary conditions are discussed further on.

The following remarks can be made with respect to the macro-micro scale transition:

- From equation (6) and (14) it appears that the microfluctuation field only enters the kinematics relative to $\vec{w}_1$ in point 1, i.e. through $\vec{w}-\vec{w}_1$. Taking the microfluctuation field in this point $\vec{w}_1$ equal to zero will not influence the obtained solution, since the averaging theorem remains valid. The only difference resides in the resulting vector $\vec{x}_c$, which is entirely determined from the coarse scale, i.e. $\vec{x}_c = \vec{c}$ see equation (8). Clearly, $\vec{x}_c$ no longer represents the deformed position of the original RVE centre $\vec{X}_c$, since it is translated with respect to this position. The choice $\vec{w}_1 = \vec{0}$ is often made in practical implementations of the first-order homogenization scheme, since it leads to the correct solution in a practical way.
- For the first-order case, any base point could have been taken to expand $\vec{x}$ according to (4) into the RVE, leading to the same solution as the specific choice made here (the RVE center $\vec{X}_c$).

- Logically, the solution does not depend on the point that was fixed at the boundary. A point inside the volume V_0 can be taken as well to eliminate rigid body displacements in (6). Again the deformed shape of the RVE and the stress state extracted from it, remain the same.

3.4 Micro-scale RVE boundary conditions

As emphasized in the previous section, possible RVE boundary conditions naturally result from the constraint (14) imposed by the scale transition. Among the various choices possible, only three particular cases will be considered hereafter in more detail. Note that the Taylor assumption trivially satisfies (14) since the microfluctuation field is then zero in the entire volume V_0 and hence also at its boundary Γ_0.

Displacement boundary conditions The first case considered is defined by constraining each point at the RVE boundary through the macroscopic deformation by

$$\vec{x} = \mathbf{F}_{\mathrm{M}} \cdot \vec{X} \quad \text{with} \quad \vec{X} \quad \text{on} \quad \Gamma_0, \tag{15}$$

This simply implies that the micro-fluctuation field $\vec{w}$ is zero at the boundary Γ_0, which trivially satisfies (14). The position of all points at the boundary are determined through the macroscopic deformation only, leading to a linear mapping of the RVE boundary. The boundary will therefore reproduce typical stretch (tension/compression) and shear modes only.

Traction boundary conditions This case departs from the assumption that $\mathbf{P}_{\mathrm{M}}$ is to be prescribed to the RVE. The boundary conditions are then defined by constraining all tractions at the RVE boundary to the macroscopic stress tensor by

$$\vec{t} = \vec{n} \cdot \boldsymbol{\sigma}_{\mathrm{M}} \quad \text{on} \quad \Gamma, \qquad \text{or} \qquad \vec{p} = \vec{N} \cdot \mathbf{P}^c_{\mathrm{M}} \quad \text{on} \quad \Gamma_0, \tag{16}$$

with $\vec{n}$ the normal to the current (Γ) RVE boundary. Note that the traction boundary conditions (16) do not completely define the microstructural boundary value problem, since rotations are yet undetermined. As emphasized earlier, these boundary conditions are a priori not appropriate in a deformation driven procedure as pursued in the present computational homogenization scheme. The interested reader is referred to the work of Miehe (2002, 2003), where it is shown that the traction boundary condition is the weakest condition to enforce (14). From a practical point of view, these boundary conditions generally yield unsatisfactory results. Therefore, the RVE traction boundary conditions will not be explored further in this chapter.

Periodic boundary conditions Making use of the earlier introduced concept of local periodicity, periodic boundary conditions are next introduced. The periodicity conditions for the microstructural RVE are written in a general format as

$$\vec{x}^{\,+} - \vec{x}^{\,-} = \mathbf{F}_{\mathrm{M}} \cdot (\vec{X}^{+} - \vec{X}^{-}), \tag{17}$$

or formulated in terms of the micro-fluctuation fields

$$\vec{w}^{\,+} \;=\; \vec{w}^{\,-} \tag{18}$$

Deformations are periodic since micro-fluctuations on opposite sides are identical. Here the (opposite) parts of the RVE boundary Γ_0^- and Γ_0^+ are defined such that $\vec{N}^- = -\vec{N}^+$ at corresponding points on Γ_0^- and Γ_0^+, see figure 4. The periodicity condition (17), being prescribed on an initially periodic RVE, preserves the periodicity of the RVE in the deformed state.

The periodic boundary conditions (17) clearly satisfy the constraint (14). This is easily observed by splitting the RVE boundary into the parts Γ_0^+ and Γ_0^-

$$\begin{aligned} \int_{\Gamma_0} \vec{w} \vec{N} d\Gamma_0 \;&=\; \int_{\Gamma_0^+} \vec{w}^{+} \vec{N}^{+} d\Gamma_0^+ + \int_{\Gamma_0^-} \vec{w}^{-} \vec{N}^{-} d\Gamma_0^- \\ &= \int_{\Gamma_0^+} \vec{w}^{+} \vec{N}^{+} d\Gamma_0^+ - \int_{\Gamma_0^-} \vec{w}^{+} \vec{N}^{+} d\Gamma_0^- \\ &= \mathbf{0} \end{aligned} \tag{19}$$

Note that as a result of microstructural equilibrium, tractions will be anti-periodic on opposite sides:

$$\vec{p}^{\,+} \;=\; -\vec{p}^{\,-}, \tag{20}$$

Note that, as has been observed by several authors (e.g. van der Sluis et al. (2000); Terada et al. (2000)), periodic boundary conditions provide a better estimation of the overall properties, than the prescribed displacement or prescribed traction boundary conditions.

4 The macro-scale problem

4.1 The micro-macro scale transition

Once the micro-scale problem has been solved, macroscopic quantities have to be extracted from the obtained results. Whereas deformation averaging was the key assumption for the macro-micro transition, energy averaging constitutes the key assumption for the reverse transition. This energy

averaging theorem, known in the literature as the Hill-Mandel condition or macro-homogeneity condition Hill (1963); Suquet (1985), requires that the macroscopic volume average of the variation of work performed on the RVE is equal to the local variation of the work on the macro-scale, i.e.

$$\delta W_{0\mathrm{M}} \;=\; \delta W_{0\mathrm{m}} \tag{21}$$

Formulated in terms of a work conjugated set, i.e. the deformation gradient tensor and the first Piola-Kirchhoff stress tensor, the Hill-Mandel condition reads

$$\underbrace{\mathbf{P}_{\mathrm{M}} : \delta\mathbf{F}^{c}_{\mathrm{M}}}_{\delta W_{0\mathrm{M}}} \;=\; \underbrace{\frac{1}{V_0}\int_{V_0} \mathbf{P}_{\mathrm{m}} : \delta\mathbf{F}^{c}_{\mathrm{m}}\,\mathrm{d}V_0}_{\delta W_{0\mathrm{m}}} \tag{22}$$

The averaged microstructural work in the right-hand side of (22) may be expressed in terms of RVE boundary quantities

$$\delta W_{0\mathrm{m}} = \frac{1}{V_0}\int_{V_0} \mathbf{P}_{\mathrm{m}} : \delta\mathbf{F}^{c}_{\mathrm{m}}\,\mathrm{d}V_0 = \frac{1}{V_0}\int_{\Gamma_0} \vec{p}\cdot\delta\vec{x}\;\mathrm{d}\Gamma_0, \tag{23}$$

where the relation (with account for microstructural equilibrium)

$$\mathbf{P}_{\mathrm{m}} : \nabla_{0\mathrm{m}}\delta\vec{x} = \nabla_{0\mathrm{m}}\cdot(\mathbf{P}^{c}_{\mathrm{m}}\cdot\delta\vec{x}) - (\nabla_{0\mathrm{m}}\cdot\mathbf{P}^{c}_{\mathrm{m}})\cdot\delta\vec{x} = \nabla_{0\mathrm{m}}\cdot(\mathbf{P}^{c}_{\mathrm{m}}\cdot\delta\vec{x}),$$

and the divergence theorem have been used.

As will be shown next, an important result of postulating the Hill-Mandel condition for an RVE with kinematic boundary conditions (fully prescribed or periodically tied), is the fact that the macroscopic stress tensor $\mathbf{P}_{\mathrm{M}}$ equals the volume average $\bar{\mathbf{P}}_{\mathrm{m}}$ of the microscopic stress tensors. To this purpose, it is convenient to establish the boundary relation for the mean RVE stress $\bar{\mathbf{P}}_{\mathrm{m}}$, i.e.

$$\begin{aligned}
\bar{\mathbf{P}}_{\mathrm{m}} \;&=\; \frac{1}{V_0}\int_{V_0} \mathbf{P}_{\mathrm{m}}\mathrm{d}V_0 \\
&=\; \frac{1}{V_0}\int_{V_0} \vec{\nabla}_0\cdot(\mathbf{P}^{c}_{\mathrm{m}}\,\vec{X})\,\mathrm{d}V_0 \\
&=\; \frac{1}{V_0}\int_{\Gamma_0} \vec{N}\cdot(\mathbf{P}^{c}_{\mathrm{m}}\,\vec{X})\,\mathrm{d}\Gamma_0 \\
&=\; \frac{1}{V_0}\int_{\Gamma_0} \vec{p}\,\vec{X}\,\mathrm{d}\Gamma_0
\end{aligned} \tag{24}$$

Displacement boundary conditions In case of fully prescribed boundary displacements (15), substitution of the variation of the boundary position vectors $\delta\vec{x} = \delta\mathbf{F}_{\mathrm{M}}{\cdot}\vec{X}$ into the expression for the averaged microwork (23) with incorporation of (33) gives

$$\delta W_{0\mathrm{m}} = \frac{1}{V_0}\int_{\Gamma_0} \vec{p}{\cdot}(\delta\mathbf{F}_{\mathrm{M}}{\cdot}\vec{X})\,\mathrm{d}\Gamma_0 = \left[\frac{1}{V_0}\int_{\Gamma_0} \vec{p}\vec{X}\,\mathrm{d}\Gamma_0\right] : \delta\mathbf{F}^c_{\mathrm{M}} = \bar{\mathbf{P}}_{\mathrm{m}} : \delta\mathbf{F}^c_{\mathrm{M}} \tag{25}$$

Enforcing the Hill-Mandel condition (22) thus implies that

$$\mathbf{P}_{\mathrm{M}} \;=\; \bar{\mathbf{P}}_{\mathrm{m}} \tag{26}$$

Traction boundary conditions Substitution of the traction boundary condition (16) into (23), with account for the variation of the average of the microscopic deformation gradient tensor obtained by varying relation (9), leads to

$$\delta W_{0\mathrm{m}} = \frac{1}{V_0}\int_{\Gamma_0} (\vec{N}{\cdot}\mathbf{P}^c_{\mathrm{M}}){\cdot}\delta\vec{x}\,\mathrm{d}\Gamma_0 = \mathbf{P}_{\mathrm{M}} : \left[\frac{1}{V_0}\int_{\Gamma_0} \vec{N}\delta\vec{x}\,\mathrm{d}\Gamma_0\right] = \mathbf{P}_{\mathrm{M}} : \delta\bar{\mathbf{F}}^c_{\mathrm{m}}. \tag{27}$$

In this case, the Hill-Mandel condition (22) enforces the resulting macroscopic deformation gradient to be taken as the volume average of the microscopic deformation gradients, i.e..

$$\mathbf{F}_{\mathrm{M}} \;=\; \bar{\mathbf{F}}_{\mathrm{m}} \;=\; \frac{1}{V_0}\int_{V_0} \mathbf{F}_{\mathrm{m}}\mathrm{d}V_0 \tag{28}$$

This implies that the traction boundary conditions, complemented by the Hill-Mandel conditions, constitute the weakest kinematic constraint for the boundary displacements, i.e. equation (14). Computing the volume average

of the micro-scale RVE stresses from equation (24) now yields

$$\begin{aligned}
\bar{\mathbf{P}}_{\mathrm{m}} &= \frac{1}{V_0}\int_{\Gamma_0} \vec{p}\,\vec{X}\,\mathrm{d}\Gamma_0 \\
&= \frac{1}{V_0}\int_{\Gamma_0} (\vec{N}\cdot\mathbf{P}^c_{\mathrm{M}})\,\vec{X}\,\mathrm{d}\Gamma_0 \\
&= \mathbf{P}_{\mathrm{M}}\cdot\left[\frac{1}{V_0}\int_{\Gamma_0} \vec{N}\vec{X}\,\mathrm{d}\Gamma_0\right] \\
&= \mathbf{P}_{\mathrm{M}}\cdot\left[\frac{1}{V_0}V_0\,\mathbf{I}\right] \\
&= \mathbf{P}_{\mathrm{M}}
\end{aligned} \tag{29}$$

Again, the macroscopic stress equals the volume average of the microscopic stress, but this time this conclusion does not result from the Hill-Mandel condition.

Periodic boundary conditions For the periodic boundary conditions (17) and the resulting anti-periodic tractions (20)

$$\begin{aligned}
\delta W_{0\mathrm{m}} &= \frac{1}{V_0}\left\{\int_{\Gamma_0^+} \vec{p}^{\,+}\cdot\delta\vec{x}^{\,+}\,\mathrm{d}\Gamma_0 + \int_{\Gamma_0^-} \vec{p}^{\,-}\cdot\delta\vec{x}^{\,-}\,\mathrm{d}\Gamma_0\right\} \\
&= \frac{1}{V_0}\int_{\Gamma_0^+} \vec{p}^{\,+}\cdot(\delta\vec{x}^{\,+} - \delta\vec{x}^{\,-})\,\mathrm{d}\Gamma_0^+ \\
&= \left[\frac{1}{V_0}\int_{\Gamma_0^+} \vec{p}^{\,+}(\vec{X}^{+} - \vec{X}^{-})\,\mathrm{d}\Gamma_0^+\right] : \delta\mathbf{F}^c_{\mathrm{M}} = \left[\frac{1}{V_0}\int_{\Gamma_0} \vec{p}\vec{X}\,\mathrm{d}\Gamma_0\right] : \delta\mathbf{F}^c_{\mathrm{M}} \\
&= \bar{\mathbf{P}}_{\mathrm{m}} : \delta\mathbf{F}^c_{\mathrm{M}}
\end{aligned} \tag{30}$$

Enforcing the Hill-Mandel condition (22) again implies that

$$\mathbf{P}_{\mathrm{M}} = \bar{\mathbf{P}}_{\mathrm{m}} \tag{31}$$

4.2 Macroscopic stress tensors

Since the scale transition implies stress averaging for all considered boundary conditions, the macroscopic stress tensor is given by

$$\mathbf{P}_{\mathrm{M}} = \frac{1}{V_0}\int_{V_0} \mathbf{P}_{\mathrm{m}}\mathrm{d}V_0 \tag{32}$$

$$= \frac{1}{V_0}\int_{\Gamma_0} \vec{p}\,\vec{X}\,\mathrm{d}\Gamma_0 \tag{33}$$

The volume average of the microscopic Cauchy stress tensor $\boldsymbol{\sigma}_{\mathrm{m}}$ over the current RVE volume V can be elaborated similarly to (33)

$$\boldsymbol{\sigma}^*_{\mathrm{M}} = \frac{1}{V}\int_{V} \boldsymbol{\sigma}_{\mathrm{m}}\,\mathrm{d}V = \frac{1}{V}\int_{\Gamma} \vec{t}\,\vec{x}\,\mathrm{d}\Gamma. \tag{34}$$

Just as it is the case for kinematic quantities, the usual pull-back push-forward relations between stress measures (e.g. the Cauchy and the first Piola-Kirchhoff stress tensors) are, in general, not valid for the volume averages of the microstructural counterparts $\boldsymbol{\sigma}^*_{\mathrm{M}} \neq \mathbf{P}_{\mathrm{M}}\cdot\mathbf{F}^c_{\mathrm{M}}/\det(\mathbf{F}_{\mathrm{M}})$. If the averaging is based on $\mathbf{P}_{\mathrm{M}}$, the Cauchy stress tensor on the macrolevel should be defined as

$$\boldsymbol{\sigma}_{\mathrm{M}} = \frac{1}{\det(\mathbf{F}_{\mathrm{M}})}\mathbf{P}_{\mathrm{M}}\cdot\mathbf{F}^c_{\mathrm{M}}. \tag{35}$$

Clearly, there is some arbitrariness in the choice of the governing deformation and stress tensors, whose macroscopic measures are equal to the volume average of their microscopic counterparts (through the imposed scale transition relations). Macroscopic measures defined on another configuration are then expressed in terms of the governing averaged quantities using the standard pull-back push-forward relations. The specific selection made here is mainly based on its ease of implementation. The actual choice of the "primary" averaging measures used here, i.e. the deformation gradient tensor $\mathbf{F}$ and the first Piola-Kirchhoff stress tensor $\mathbf{P}$ (and their rates), has been advocated in Miehe et al. (1999b); Hill (1984); Nemat-Nasser (1999) (in the last two references the nominal stress $\mathbf{S}_N = \det(\mathbf{F})\mathbf{F}^{-1}\cdot\boldsymbol{\sigma} = \mathbf{P}^c$ has been used). This particular choice is motivated by the fact that these two measures are work conjugated, combined with the observation that their volume averages can exclusively be defined in terms of the microstructural quantities of the undeformed RVE boundary.

5 Two-scale numerical solution strategy

Once the boundary conditions have been properly defined through one of the methods outline above and once all phases in the microstructure have been characterized, a standard boundary value problem (BVP) has been obtained. The solution of this BVP follows standard procedures. In the present computational homogenization method, it will be assumed that the finite element method has been used to this purpose. The solution of this BVP problem automatically leads to the proper determination of all position vectors in the RVE and all tractions along its boundary. The analysis is further restricted to kinematic RVE boundary conditions only.

5.1 RVE boundary value problem

The RVE problem to be solved is a standard non-linear quasi-static boundary value problem with kinematic boundary conditions. Following the standard finite element procedure for the microlevel RVE, after discretization, the weak form of equilibrium (2) with account for the constitutive relations (3) leads to a system of non-linear algebraic equations in the unknown nodal displacements $\underset{\sim}{u}$

$$\underset{\sim}{f}_{int}(\underset{\sim}{u}) = \underset{\sim}{f}_{ext}, \tag{36}$$

expressing the balance of internal and external nodal forces. This system has to be completed by the governing boundary conditions. To this purpose, the earlier introduced kinematic boundary conditions (15) or (17) will be elaborated in more detail.

Fully prescribed boundary displacements In the case of the fully prescribed displacement boundary conditions (15), the displacements of all nodes on the boundary is simply given by

$$\vec{u}_p = (\mathbf{F}_{\mathrm{M}} - \mathbf{I})\cdot\vec{X}_p, \qquad p = \overline{1, N_p} \tag{37}$$

where N_p is the number of prescribed nodes, which in this case simply equals to the number of boundary nodes. The boundary conditions (37) are simply added to the system (36) in a standard manner by static condensation, Lagrange multipliers or penalty functions.

Periodic boundary conditions Prior to the incorporation of the periodic boundary conditions (17), they have to be rewritten into a format that is more suitable for a finite element framework. Consider a two-dimensional periodic RVE schematically depicted in figure 4. The boundary of this RVE

can be split into four parts, here denoted as "T" top, "B" bottom, "R" right and "L" left. To ease application of the periodicity constraint, a finite element discretization is next considered which has a periodic distribution of nodes on opposite edges. Exploiting the initial periodicity of the RVE (in its reference configuration) allows to write for every respective pair of nodes on the top-bottom and right-left boundaries:

$$\begin{aligned} \vec{X}_{\mathrm{T}} - \vec{X}_{\mathrm{B}} &= \vec{X}_4 - \vec{X}_1, \\ \vec{X}_{\mathrm{R}} - \vec{X}_{\mathrm{L}} &= \vec{X}_2 - \vec{X}_1, \end{aligned} \tag{38}$$

where $\vec{X}_p,\ p = 1, 2, 4$ are the position vectors of the corner nodes 1, 2 and 4 in the undeformed state. Considering pairs of periodic nodes on opposite boundaries, allows to express (17) as

$$\begin{aligned} \vec{x}_{\mathrm{T}} - \vec{x}_{\mathrm{B}} &= \mathbf{F}_{\mathrm{M}} \cdot (\vec{X}_4 - \vec{X}_1), \\ \vec{x}_{\mathrm{R}} - \vec{x}_{\mathrm{L}} &= \mathbf{F}_{\mathrm{M}} \cdot (\vec{X}_2 - \vec{X}_1). \end{aligned} \tag{39}$$

Applying these relations to the four corner nodes, permits to conclude that the position vectors of the corner nodes in the deformed state are in fact prescribed according to

$$\vec{x}_p = \mathbf{F}_{\mathrm{M}} \cdot \vec{X}_p, \qquad p = 1, 2, 4 \tag{40}$$

The periodic boundary conditions may finally be rewritten as

$$\begin{aligned} \vec{x}_{\mathrm{T}} &= \vec{x}_{\mathrm{B}} + \vec{x}_4 - \vec{x}_1, \\ \vec{x}_{\mathrm{R}} &= \vec{x}_{\mathrm{L}} + \vec{x}_2 - \vec{x}_1. \end{aligned} \tag{41}$$

Since these conditions are trivially satisfied in the undeformed configuration, they may be formulated in terms of displacements

$$\begin{aligned} \vec{u}_{\mathrm{T}} &= \vec{u}_{\mathrm{B}} + \vec{u}_4 - \vec{u}_1, \\ \vec{u}_{\mathrm{R}} &= \vec{u}_{\mathrm{L}} + \vec{u}_2 - \vec{u}_1, \end{aligned} \tag{42}$$

whereby

$$\vec{u}_p = (\mathbf{F}_{\mathrm{M}} - \mathbf{I}) \cdot \vec{X}_p, \qquad p = 1, 2, 4 \tag{43}$$

In a discretized format the relations (42) lead to a set of homogeneous constraints of the type

$$\underline{C}_a \, \underset{\sim}{u}_a = \underline{0}, \tag{44}$$

with $\underline{C}_a$ a matrix containing coefficients in the constraint relations and $\underset{\sim}{u}_a$ a column with the degrees of freedom involved in the constraints. Procedures

for imposing constraints (44) include the direct elimination of the dependent degrees of freedom from the system of equations, or the use of Lagrange multipliers or penalty functions. In the following, constraints (44) are enforced by elimination of the dependent degrees of freedom. Although such a procedure may be found in many textbooks on finite elements (e.g. Cook et al. (1989)), it is here summarized for the sake of clarity and completeness, since it will be applied in section 5.3 for the derivation of the macroscopic tangent stiffness.

To this purpose, the homogeneous constraint relations (44) are partitioned according to

$$[\underline{C}_i \quad \underline{C}_d] \left[\begin{array}{c} \underset{\sim}{u}_i \\ \underset{\sim}{u}_d \end{array} \right] = \underset{\sim}{0}, \tag{45}$$

where $\underset{\sim}{u}_i$ are the independent degrees of freedom (to be retained in the system) and $\underset{\sim}{u}_d$ are the dependent degrees of freedom (to be eliminated from the system). Because there are as many dependent degrees of freedom $\underset{\sim}{u}_d$ as there are independent constraint equations in (45), matrix $\underline{C}_d$ is square and non-singular. Solution for $\underset{\sim}{u}_d$ yields

$$\underset{\sim}{u}_d = \underline{C}_{di}\, \underset{\sim}{u}_i, \qquad \text{with} \quad \underline{C}_{di} = -\underline{C}_d^{-1} \underline{C}_i. \tag{46}$$

This relation may be further rewritten as

$$\left[\begin{array}{c} \underset{\sim}{u}_i \\ \underset{\sim}{u}_d \end{array} \right] = \underline{T}\, \underset{\sim}{u}_i, \qquad \text{with} \quad \underline{T} = \left[\begin{array}{c} \underline{I} \\ \underline{C}_{di} \end{array} \right], \tag{47}$$

where $\underline{I}$ is a unit matrix of size $[N_i \times N_i]$, with N_i the number of the independent degrees of freedom.

With the transformation matrix $\underline{T}$ defined such that $\underset{\sim}{d} = \underline{T}\, \underset{\sim}{d}'$, the common transformations $\underset{\sim}{r}' = \underline{T}^T \underset{\sim}{r}$ and $\underline{K}' = \underline{T}^T \underline{K} \underline{T}$ can be applied to a linear system of equations of the form $\underline{K}\, \underset{\sim}{d} = \underset{\sim}{r}$, leading to a new system $\underline{K}'\, \underset{\sim}{d}' = \underset{\sim}{r}'$.

The standard linearization of the non-linear system of equations (36) leads to a linear system in the iterative corrections $\delta \underset{\sim}{u}$ to the current estimate $\underset{\sim}{u}$. This system may be partitioned as

$$\left[\begin{array}{cc} \underline{K}_{ii} & \underline{K}_{id} \\ \underline{K}_{di} & \underline{K}_{dd} \end{array} \right] \left[\begin{array}{c} \delta \underset{\sim}{u}_i \\ \delta \underset{\sim}{u}_d \end{array} \right] = \left[\begin{array}{c} \delta \underset{\sim}{r}_i \\ \delta \underset{\sim}{r}_d \end{array} \right], \tag{48}$$

with the residual nodal forces at the right-hand side. Noting that all the constraint equations considered above are linear, and thus their linearization is straightforward, application of the transformation (47) to the system (48) gives

$$\left[\underline{K}_{ii} + \underline{K}_{id} \underline{C}_{di} + \underline{C}_{di}^T \underline{K}_{di} + \underline{C}_{di}^T \underline{K}_{dd} \underline{C}_{di} \right] \delta \underset{\sim}{u}_i = \left[\delta \underset{\sim}{r}_i + \underline{C}_{di}^T \delta \underset{\sim}{r}_d \right]. \tag{49}$$

Note that the boundary conditions (43) prescribing displacements of the corner nodes have not yet been applied. The column of "independent" degrees of freedom $\underset{\sim}{u}_i$ includes the prescribed corner nodes $\underset{\sim}{u}_p$ among other nodes. The boundary conditions (43) should be applied to the system (49) is a standard manner.

The condition of antiperiodic tractions (20) will be addressed in section 5.2.

5.2 Extraction of the macroscopic stress

After the analysis of a microstructural RVE is completed, the RVE averaged stress have to be extracted. Of course, the macroscopic stress tensor can be calculated by numerically evaluating the volume integral (32). However it is computationally more efficient to compute the boundary integral (33), which can be further simplified for the case of the periodic boundary conditions.

Fully prescribed boundary displacements For the case of prescribed displacement boundary conditions the boundary integral (33) simply leads to

$$\mathbf{P}_{\mathrm{M}} = \frac{1}{V_0} \sum_{p=1}^{N_p} \vec{f}_p \vec{X}_p, \tag{50}$$

where $\vec{f}_p$ are the resulting external forces at the boundary nodes and $\vec{X}_p$ the position vectors of these nodes in the undeformed state; N_p is the number of the nodes on the boundary.

Periodic boundary conditions In order to simplify the boundary integral (33) for the case of periodic boundary conditions, consider all the forces acting on the RVE boundary subjected to the boundary conditions according to (42)–(43). At the three prescribed corner nodes the resulting external forces $\vec{f}^{\mathrm{e}}_p$, $p = 1, 2, 4$ act. Additionally, there are forces involved in every constraint (tying) relation (42). For example, for each constraint relation between pairs of the nodes on the bottom-top boundaries there is a tying force at the node on the bottom boundary $\vec{p}^{\,\mathrm{t}}_{\mathrm{B}}$, a tying force at the node on the top boundary $\vec{p}^{\,\mathrm{t}}_{\mathrm{T}}$ and tying forces at the corner nodes 1 and 4, $\vec{p}^{\,\mathrm{t_B}}_1$ and $\vec{p}^{\,\mathrm{t_B}}_4$, respectively. Similarly there are forces $\vec{p}^{\,\mathrm{t}}_{\mathrm{L}}$, $\vec{p}^{\,\mathrm{t}}_{\mathrm{R}}$, $\vec{p}^{\,\mathrm{t_L}}_1$ and $\vec{p}^{\,\mathrm{t_L}}_2$ corresponding to the left-right constraints. All these forces are schematically shown in figure 5.

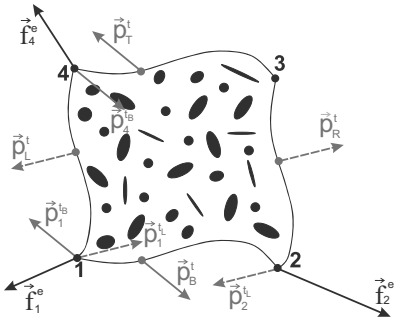

Figure 5. Tractions acting on the boundary of a two-dimensional RVE subjected to periodic boundary conditions.

Each constraint relation satisfies the condition of zero virtual work, i.e.

$$\begin{aligned}\vec{p}^{\,\mathrm{t}}_{\mathrm{B}}\cdot\delta\vec{x}_{\mathrm{B}} + \vec{p}^{\,\mathrm{t}}_{\mathrm{T}}\cdot\delta\vec{x}_{\mathrm{T}} + \vec{p}^{\,\mathrm{t_B}}_{1}\cdot\delta\vec{x}_{1} + \vec{p}^{\,\mathrm{t_B}}_{4}\cdot\delta\vec{x}_{4} = 0,\\ \vec{p}^{\,\mathrm{t}}_{\mathrm{L}}\cdot\delta\vec{x}_{\mathrm{L}} + \vec{p}^{\,\mathrm{t}}_{\mathrm{R}}\cdot\delta\vec{x}_{\mathrm{R}} + \vec{p}^{\,\mathrm{t_L}}_{1}\cdot\delta\vec{x}_{1} + \vec{p}^{\,\mathrm{t_L}}_{2}\cdot\delta\vec{x}_{2} = 0.\end{aligned} \tag{51}$$

Substitution of the variation of the constraints (41) into (51) gives

$$\begin{aligned}(\vec{p}^{\,\mathrm{t}}_{\mathrm{B}} + \vec{p}^{\,\mathrm{t}}_{\mathrm{T}})\cdot\delta\vec{x}_{\mathrm{B}} + (\vec{p}^{\,\mathrm{t_B}}_{1} - \vec{p}^{\,\mathrm{t}}_{\mathrm{T}})\cdot\delta\vec{x}_{1} + (\vec{p}^{\,\mathrm{t}}_{\mathrm{T}} + \vec{p}^{\,\mathrm{t_B}}_{4})\cdot\delta\vec{x}_{4} = 0,\\ (\vec{p}^{\,\mathrm{t}}_{\mathrm{L}} + \vec{p}^{\,\mathrm{t}}_{\mathrm{R}})\cdot\delta\vec{x}_{\mathrm{L}} + (\vec{p}^{\,\mathrm{t_L}}_{1} - \vec{p}^{\,\mathrm{t}}_{\mathrm{R}})\cdot\delta\vec{x}_{1} + (\vec{p}^{\,\mathrm{t}}_{\mathrm{R}} + \vec{p}^{\,\mathrm{t_L}}_{2})\cdot\delta\vec{x}_{2} = 0.\end{aligned} \tag{52}$$

These relations should hold for any $\delta\vec{x}_{\mathrm{B}}$, $\delta\vec{x}_{\mathrm{L}}$, $\delta\vec{x}_{1}$, $\delta\vec{x}_{2}$, $\delta\vec{x}_{4}$, therefore

$$\begin{aligned}\vec{p}^{\,\mathrm{t}}_{\mathrm{B}} = -\vec{p}^{\,\mathrm{t}}_{\mathrm{T}} = -\vec{p}^{\,\mathrm{t_B}}_{1} = \vec{p}^{\,\mathrm{t_B}}_{4},\\ \vec{p}^{\,\mathrm{t}}_{\mathrm{L}} = -\vec{p}^{\,\mathrm{t}}_{\mathrm{R}} = -\vec{p}^{\,\mathrm{t_L}}_{1} = \vec{p}^{\,\mathrm{t_L}}_{2}.\end{aligned} \tag{53}$$

Equation (53) reflects the antiperiodicity of tying forces on the opposite boundaries, which has been introduced previously in equation (20).

With account for all forces acting on the RVE boundary, the boundary integral (33) is written as

$$\begin{aligned}\mathbf{P}_{\mathrm{M}} = \frac{1}{V_0}\Bigg(&\vec{f}^{\,\mathrm{e}}_{1}\vec{X}_1 + \vec{f}^{\,\mathrm{e}}_{2}\vec{X}_2 + \vec{f}^{\,\mathrm{e}}_{4}\vec{X}_4 + \int_{\Gamma_{0\mathrm{B}}} \vec{p}^{\,\mathrm{t}}_{\mathrm{B}}\vec{X}_{\mathrm{B}}\,\mathrm{d}\Gamma_0 + \int_{\Gamma_{0\mathrm{T}}} \vec{p}^{\,\mathrm{t}}_{\mathrm{T}}\vec{X}_{\mathrm{T}}\,\mathrm{d}\Gamma_0 +\\ &\int_{\Gamma_{0\mathrm{L}}} \vec{p}^{\,\mathrm{t}}_{\mathrm{L}}\vec{X}_{\mathrm{L}}\,\mathrm{d}\Gamma_0 + \int_{\Gamma_{0\mathrm{R}}} \vec{p}^{\,\mathrm{t}}_{\mathrm{R}}\vec{X}_{\mathrm{R}}\,\mathrm{d}\Gamma_0 + \Big(\int_{\Gamma_{0\mathrm{B}}} \vec{p}^{\,\mathrm{t_B}}_{1}\,\mathrm{d}\Gamma_0\Big)\vec{X}_1 +\\ &\Big(\int_{\Gamma_{0\mathrm{L}}} \vec{p}^{\,\mathrm{t_L}}_{1}\,\mathrm{d}\Gamma_0\Big)\vec{X}_1 + \Big(\int_{\Gamma_{0\mathrm{B}}} \vec{p}^{\,\mathrm{t_B}}_{4}\,\mathrm{d}\Gamma_0\Big)\vec{X}_4 + \Big(\int_{\Gamma_{0\mathrm{L}}} \vec{p}^{\,\mathrm{t_L}}_{2}\,\mathrm{d}\Gamma_0\Big)\vec{X}_2\Bigg).\end{aligned} \tag{54}$$

Making use of the relation between tying forces (53) gives

$$\mathbf{P}_{\mathrm{M}} = \frac{1}{V_0}\Big(\sum_{p=1,2,4} \vec{f}^{\,\mathrm{e}}_p \vec{X}_p + \int_{\Gamma_{0\mathrm{B}}} \vec{p}^{\,\mathrm{t}}_{\mathrm{B}} (\vec{X}_{\mathrm{B}} - \vec{X}_{\mathrm{T}})\, \mathrm{d}\Gamma_0 + \int_{\Gamma_{0\mathrm{L}}} \vec{p}^{\,\mathrm{t}}_{\mathrm{L}} (\vec{X}_{\mathrm{L}} - \vec{X}_{\mathrm{R}})\, \mathrm{d}\Gamma_0 + \big(\int_{\Gamma_{0\mathrm{B}}} \vec{p}^{\,\mathrm{t}_{\mathrm{B}}}_1\, \mathrm{d}\Gamma_0 \big) \vec{X}_1 + \big(\int_{\Gamma_{0\mathrm{L}}} \vec{p}^{\,\mathrm{t}_{\mathrm{L}}}_1\, \mathrm{d}\Gamma_0 \big) \vec{X}_1 + \big(\int_{\Gamma_{0\mathrm{B}}} \vec{p}^{\,\mathrm{t}_{\mathrm{B}}}_4\, \mathrm{d}\Gamma_0 \big) \vec{X}_4 + \big(\int_{\Gamma_{0\mathrm{L}}} \vec{p}^{\,\mathrm{t}_{\mathrm{L}}}_2\, \mathrm{d}\Gamma_0 \big) \vec{X}_2 \Big). \tag{55}$$

Inserting the conditions of the initial periodicity of the RVE (38) results in

$$\mathbf{P}_{\mathrm{M}} = \frac{1}{V_0}\Big(\sum_{p=1,2,4} \vec{f}^{\,\mathrm{e}}_p \vec{X}_p + \int_{\Gamma_{0\mathrm{B}}} (\vec{p}^{\,\mathrm{t}}_{\mathrm{B}} + \vec{p}^{\,\mathrm{t}_{\mathrm{B}}}_1) \vec{X}_1\, \mathrm{d}\Gamma_0 + \int_{\Gamma_{0\mathrm{L}}} (\vec{p}^{\,\mathrm{t}}_{\mathrm{L}} + \vec{p}^{\,\mathrm{t}_{\mathrm{L}}}_1) \vec{X}_1\, \mathrm{d}\Gamma_0 + \int_{\Gamma_{0\mathrm{B}}} (\vec{p}^{\,\mathrm{t}_{\mathrm{B}}}_4 - \vec{p}^{\,\mathrm{t}}_{\mathrm{B}}) \vec{X}_4\, \mathrm{d}\Gamma_0 + \int_{\Gamma_{0\mathrm{L}}} (\vec{p}^{\,\mathrm{t}_{\mathrm{L}}}_2 - \vec{p}^{\,\mathrm{t}}_{\mathrm{L}}) \vec{X}_2\, \mathrm{d}\Gamma_0 \Big), \tag{56}$$

which after substitution of the remaining relations between tying forces (53) gives

$$\mathbf{P}_{\mathrm{M}} = \frac{1}{V_0} \sum_{p=1,2,4} \vec{f}^{\,\mathrm{e}}_p \vec{X}_p. \tag{57}$$

Therefore, when the periodic boundary conditions are used, all the terms with forces involved into the periodicity constraints cancel out from the boundary integral (33) and the only contribution left is by the external forces at the three prescribed corner nodes.

5.3 Extraction of the macroscopic tangent operator

When the micro-macro approach is implemented within the framework of a non-linear finite element code, the stiffness matrix at every macroscopic integration point is required. Because in the computational homogenization approach there is no explicit form of the constitutive behaviour on the macrolevel assumed a priori, the stiffness matrix has to be determined numerically from the relation between variations of the macroscopic stress and variations of the macroscopic deformation at such a point. This may be realized by numerical differentiation of the numerical macroscopic stress-strain relation, for example using a forward difference approximation as has been suggested in Miehe (1996). Another approach is to condense the microstructural stiffness to the local macroscopic stiffness. This is achieved by reducing

the total RVE system of equations to the relation between the forces acting on the RVE boundary and the associated boundary displacements. Such a procedure in combination with the Lagrange multiplier method to impose boundary constraints has been elaborated in Miehe and Koch (2002). Here an alternative scheme, which employs the direct condensation of the constrained degrees of freedom, as has been presented in Kouznetsova et al. (2001); Kouznetsova (2002) will be considered. After the condensed microscopic stiffness relating the prescribed displacement and force variations is obtained, it needs to be transformed to arrive at an expression relating variations of the macroscopic stress and deformation tensors, typically used in the finite element codes. These two steps are elaborated in the following.

Condensation of the microscopic stiffness matrix: fully prescribed boundary displacements First the total microstructural system of equations (in its linearized form) is partitioned as

$$\begin{bmatrix} \underline{K}_{pp} & \underline{K}_{pf} \\ \underline{K}_{fp} & \underline{K}_{ff} \end{bmatrix} \begin{bmatrix} \delta \underset{\sim}{u}_p \\ \delta \underset{\sim}{u}_f \end{bmatrix} = \begin{bmatrix} \delta \underset{\sim}{f}_p \\ \underset{\sim}{0} \end{bmatrix}, \tag{58}$$

where $\delta \underset{\sim}{u}_p$ and $\delta \underset{\sim}{f}_p$ are the columns with iterative displacements and external forces of the boundary nodes, respectively, and $\delta \underset{\sim}{u}_f$ the column with the iterative displacements of the remaining (interior) nodes; $\underline{K}_{pp}$, $\underline{K}_{pf}$, $\underline{K}_{fp}$ and $\underline{K}_{ff}$ are the corresponding partitions of the total RVE stiffness matrix. The stiffness matrix in the formulation (58) is taken at the end of a microstructural increment, where a converged state is reached. Elimination of $\delta \underset{\sim}{u}_f$ from (58) leads to the reduced stiffness matrix $\underline{K}_{\mathrm{M}}$ relating boundary displacement variations to boundary force variations

$$\underline{K}_{\mathrm{M}} \delta \underset{\sim}{u}_p = \delta \underset{\sim}{f}_p, \qquad \text{with} \quad \underline{K}_{\mathrm{M}} = \underline{K}_{pp} - \underline{K}_{pf} (\underline{K}_{ff})^{-1} \underline{K}_{fp}. \tag{59}$$

Condensation of the microscopic stiffness matrix: periodic boundary conditions In the case of the periodic boundary conditions the point of departure is the microscopic system of equations (49) from which the dependent degrees of freedom have been eliminated (as described in section 5.1)

$$\underline{K}^{\star} \delta \underset{\sim}{u}_i = \delta \underset{\sim}{r}^{\star}, \tag{60}$$

$$\text{with} \qquad \underline{K}^{\star} = \underline{K}_{ii} + \underline{K}_{id} \underline{C}_{di} + \underline{C}_{di}^T \underline{K}_{di} + \underline{C}_{di}^T \underline{K}_{dd} \underline{C}_{di},$$

$$\delta \underset{\sim}{r}^{\star} = \delta \underset{\sim}{r}_i + \underline{C}_{di}^T \delta \underset{\sim}{r}_d.$$

Next, system (60) is further split, similarly to (58), into the parts corresponding to the variations of the prescribed degrees of freedom $\delta \underset{\sim}{u}_p$ (which

in this case are the varied positions of the three corner nodes prescribed according to (43)), variations of the external forces at these prescribed nodes denoted by $\delta \underset{\sim}{f}^{\star}_{p}$, and the remaining (free) displacement variations $\delta \underset{\sim}{u}_{f}$:

$$\begin{bmatrix} \underline{K}^{\star}_{pp} & \underline{K}^{\star}_{pf} \\ \underline{K}^{\star}_{fp} & \underline{K}^{\star}_{ff} \end{bmatrix} \begin{bmatrix} \delta \underset{\sim}{u}_{p} \\ \delta \underset{\sim}{u}_{f} \end{bmatrix} = \begin{bmatrix} \delta \underset{\sim}{f}^{\star}_{p} \\ \underset{\sim}{0} \end{bmatrix}. \tag{61}$$

Then the reduced stiffness matrix $\underline{K}^{\star}_{\mathrm{M}}$ in case of periodic boundary conditions is obtained as

$$\underline{K}^{\star}_{\mathrm{M}} \delta \underset{\sim}{u}_{p} = \delta \underset{\sim}{f}^{\star}_{p}, \qquad \text{with} \quad \underline{K}^{\star}_{\mathrm{M}} = \underline{K}^{\star}_{pp} - \underline{K}^{\star}_{pf} (\underline{K}^{\star}_{ff})^{-1} \underline{K}^{\star}_{fp}. \tag{62}$$

Note that $\underline{K}^{\star}_{\mathrm{M}}$ is $[6 \times 6]$ matrix only (in the two-dimensional case).

Final macroscopic tangent Finally, the resulting relation between displacement and force variations (relation (59) if prescribed displacement boundary conditions are used, or relation (62) if periodicity conditions are employed) needs to be transformed to arrive at an expression relating variations of the macroscopic stress and deformation tensors

$$\delta \mathbf{P}_{\mathrm{M}} = {}^{4}\mathbf{C}^{\mathrm{P}}_{\mathrm{M}} : \delta \mathbf{F}^{c}_{\mathrm{M}}, \tag{63}$$

where the fourth order tensor ${}^{4}\mathbf{C}^{\mathrm{P}}_{\mathrm{M}}$ represents the required consistent tangent stiffness at the macroscopic integration point level.

In order to obtain this constitutive tangent from the reduced stiffness matrix $\underline{K}_{\mathrm{M}}$ (or $\underline{K}^{\star}_{\mathrm{M}}$), first relations (59) and (62) are rewritten in a specific vector/tensor format

$$\sum_{j} \mathbf{K}^{(ij)}_{\mathrm{M}} \cdot \delta \vec{u}_{(j)} = \delta \vec{f}_{(i)}, \tag{64}$$

where indices i and j take the values $i, j = \overline{1, N_p}$ for prescribed displacement boundary conditions (N_p is the number of boundary nodes) and $i, j = 1, 2, 4$ for the periodic boundary conditions. In (64) the components of the tensors $\mathbf{K}^{(ij)}_{\mathrm{M}}$ are simply found in the tangent matrix $\underline{K}_{\mathrm{M}}$ (for displacement boundary conditions) or in the matrix $\underline{K}^{\star}_{\mathrm{M}}$ (for periodic boundary conditions) at the rows and columns of the degrees of freedom in the nodes i and j. For example, for the case of the periodic boundary conditions the total matrix

$\underline{K}^{\star}_{\mathrm{M}}$ has the format

$$\underline{K}^{\star}_{\mathrm{M}} = \begin{bmatrix} \begin{bmatrix} K_{11}^{(11)} & K_{12}^{(11)} \\ K_{21}^{(11)} & K_{22}^{(11)} \end{bmatrix} & \begin{bmatrix} K_{11}^{(12)} & K_{12}^{(12)} \\ K_{21}^{(12)} & K_{22}^{(12)} \end{bmatrix} & \begin{bmatrix} K_{11}^{(14)} & K_{12}^{(14)} \\ K_{21}^{(14)} & K_{22}^{(14)} \end{bmatrix} \\ \begin{bmatrix} K_{11}^{(21)} & K_{12}^{(21)} \\ K_{21}^{(21)} & K_{22}^{(21)} \end{bmatrix} & \begin{bmatrix} K_{11}^{(22)} & K_{12}^{(22)} \\ K_{21}^{(22)} & K_{22}^{(22)} \end{bmatrix} & \begin{bmatrix} K_{11}^{(24)} & K_{12}^{(24)} \\ K_{21}^{(24)} & K_{22}^{(24)} \end{bmatrix} \\ \begin{bmatrix} K_{11}^{(41)} & K_{12}^{(41)} \\ K_{21}^{(41)} & K_{22}^{(41)} \end{bmatrix} & \begin{bmatrix} K_{11}^{(42)} & K_{12}^{(42)} \\ K_{21}^{(42)} & K_{22}^{(42)} \end{bmatrix} & \begin{bmatrix} K_{11}^{(44)} & K_{12}^{(44)} \\ K_{21}^{(44)} & K_{22}^{(44)} \end{bmatrix} \end{bmatrix}, \tag{65}$$

where the superscripts in round brackets refer to the nodes and the subscripts to the degrees of freedom at those nodes. Then each submatrix in (65) may be considered as the representation of a second-order tensor $\mathbf{K}_{\mathrm{M}}^{(ij)}$.

Next, the expression for the variation of the nodal forces (64) is substituted into the relation for the variation of the macroscopic stress following from (50) or (57)

$$\delta\mathbf{P}_{\mathrm{M}} = \frac{1}{V_0}\sum_i\sum_j (\mathbf{K}_{\mathrm{M}}^{(ij)}\cdot\delta\vec{u}_{(j)})\vec{X}_{(i)}. \tag{66}$$

Substitution of the equation $\delta\vec{u}_{(j)} = \vec{X}_{(j)}\cdot\delta\mathbf{F}^{c}_{\mathrm{M}}$ into (66) gives

$$\delta\mathbf{P}_{\mathrm{M}} = \frac{1}{V_0}\sum_i\sum_j (\vec{X}_{(i)}\mathbf{K}_{\mathrm{M}}^{(ij)}\vec{X}_{(j)})^{LC} : \delta\mathbf{F}^{c}_{\mathrm{M}}, \tag{67}$$

where the superscript LC denotes left conjugation, which for a fourth-order tensor ${}^{4}\mathbf{T}$ is defined as $T^{LC}_{ijkl} = T_{jikl}$. Finally, by comparing (67) with (63) the consistent constitutive tangent is identified as

$${}^{4}\mathbf{C}^{\mathrm{P}}_{\mathrm{M}} = \frac{1}{V_0}\sum_i\sum_j (\vec{X}_{(i)}\mathbf{K}_{\mathrm{M}}^{(ij)}\vec{X}_{(j)})^{LC}. \tag{68}$$

If the macroscopic finite element scheme requires the constitutive tangent relating the variation of the macroscopic Cauchy stress to the variation of the macroscopic deformation gradient tensor according to

$$\delta\boldsymbol{\sigma}_{\mathrm{M}} = {}^{4}\mathbf{C}^{\sigma}_{\mathrm{M}} : \delta\mathbf{F}^{c}_{\mathrm{M}}, \tag{69}$$

this tangent may be obtained by varying the definition equation of the macroscopic Cauchy stress tensor (35), followed by substitution of (50) (or

(57)) and (67). This gives

$$\delta\boldsymbol{\sigma}_{\mathrm{M}} = \left[\frac{1}{V}\sum_i\sum_j (\vec{x}_{(i)}\mathbf{K}_{\mathrm{M}}^{(ij)}\vec{X}_{(j)})^{LC} + \frac{1}{V}\sum_i \vec{f}_{(i)}\mathbf{I}\,\vec{X}_{(i)} - \boldsymbol{\sigma}_{\mathrm{M}}\mathbf{F}_{\mathrm{M}}^{-c}\right] : \delta\mathbf{F}_{\mathrm{M}}^{c}, \tag{70}$$

where the expression in square brackets is identified as the required tangent stiffness tensor ${}^{4}\mathbf{C}_{\mathrm{M}}^{\sigma}$. In the derivation of (70) it has been used that in case of prescribed displacements of the RVE boundary (15) or of periodic boundary conditions (17), the initial and current volumes of an RVE are related according to $J_{\mathrm{M}} = \det(\mathbf{F}_{\mathrm{M}}) = V/V_0$.

5.4 Nested solution strategy

Based on the above developments the actual implementation of the computational homogenization strategy may be described by the following subsequent steps.

The macroscopic structure to be analyzed is discretized by finite elements. The external load is applied by an incremental procedure. Increments can be associated with discrete time steps. The solution of the macroscopic non-linear system of equations is performed in a standard iterative manner. To each macroscopic integration point a discretized RVE is assigned. The geometry of the RVE is based on the microstructural morphology of the material under consideration.

For each macroscopic integration point the local macroscopic deformation gradient tensor $\mathbf{F}_{\mathrm{M}}$ is computed from the iterative macroscopic nodal displacements (during the initialization step, zero deformation is assumed throughout the macroscopic structure, i.e. $\mathbf{F}_{\mathrm{M}} = \mathbf{I}$, which allows to obtain the initial macroscopic constitutive tangent). The macroscopic deformation gradient tensor is used to formulate the boundary conditions according to (37) or (42)–(43) to be applied on the corresponding representative cell.

The solution of the RVE boundary value problem employing a fine scale finite element procedure, provides the resulting stress and strain distributions in the microstructural cell. Using the resulting forces at the prescribed nodes, the RVE averaged first Piola-Kirchhoff stress tensor $\mathbf{P}_{\mathrm{M}}$ is computed according to (50) or (57) and returned to the macroscopic integration point as a local macroscopic stress. From the global RVE stiffness matrix the local macroscopic consistent tangent ${}^{4}\mathbf{C}_{\mathrm{M}}^{\mathrm{P}}$ is obtained according to (68).

When the analysis of all microstructural RVEs is finished, the stress tensor is available at every macroscopic integration point. Thus, the internal macroscopic forces can be calculated. If these forces are in balance with the external load, incremental convergence has been achieved and the next time increment can be evaluated. If there is no convergence, the pro-

cedure is continued to achieve an updated estimation of the macroscopic nodal displacements. The macroscopic stiffness matrix is assembled using the constitutive tangents available at every macroscopic integration point from the RVE analysis. The solution of the macroscopic system of equations leads to an updated estimation of the macroscopic displacement field. The solution scheme is summarized in Table 1. It is remarked that the two-level scheme outlined above can be used selectively depending on the macroscopic deformation, e.g. in the elastic domain the macroscopic constitutive tangents do not have to be updated at every macroscopic loading step.

Table 1. Incremental-iterative nested multi-scale solution scheme for the computational homogenization.

MACRO		**MICRO**
1. Initialization		
▷ initialize the macroscopic model		
▷ assign an RVE to every integration point		
▷ loop over all integration points		
set $\mathbf{F}_{\mathrm{M}} = \mathbf{I}$		Initialization RVE analysis
	$\mathbf{F}_{\mathrm{M}} \longrightarrow$	▷ prescribe boundary conditions
		▷ assemble the RVE stiffness
store the tangent	$\longleftarrow$ tangent	▷ calculate the tangent ${}^{4}\mathbf{C}_{\mathrm{M}}^{\mathrm{P}}$
▷ end integration point loop		
2. Next increment		
▷ apply increment of the macro load		
3. Next iteration		
▷ assemble the macroscopic tangent stiffness		
▷ solve the macroscopic system		
▷ loop over all integration points		
calculate $\mathbf{F}_{\mathrm{M}}$		RVE analysis
	$\mathbf{F}_{\mathrm{M}} \longrightarrow$	▷ prescribe boundary conditions
		▷ assemble the RVE stiffness
		▷ solve the RVE problem
store $\mathbf{P}_{\mathrm{M}}$	$\longleftarrow \mathbf{P}_{\mathrm{M}}$	▷ calculate $\mathbf{P}_{\mathrm{M}}$
store the tangent	$\longleftarrow$ tangent	▷ calculate the tangent ${}^{4}\mathbf{C}_{\mathrm{M}}^{\mathrm{P}}$
▷ end integration point loop		
▷ assemble the macroscopic internal forces		
4. Check for convergence		
▷ if not converged ⇒ step 3		
▷ else ⇒ step 2		

6 Example: two-scale coupled analysis in bending

As an example, the computational homogenization approach is applied to pure bending of a rectangular strip under plane strain conditions. Both the length and the height of the sample equal 0.2 m, the thickness is taken 1 m. The macromesh is composed of 5 quadrilateral 8 node plane strain reduced integration elements. The undeformed and deformed geometries of the macromesh are schematically depicted in figure 6. At the left side the strip is fixed in axial (horizontal) direction, the displacement in transverse (vertical) direction is left free. At the right side the rotation of the cross section is prescribed. As pure bending is considered the behaviour of the strip is uniform in axial direction and, therefore, a single layer of elements on the macrolevel suffices to simulate the situation.

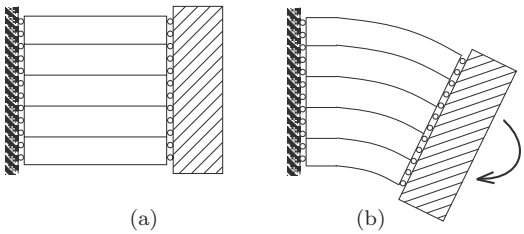

Figure 6. Schematic representation of the undeformed (a) and deformed (b) configurations of the macroscopically bended specimen.

In this example two heterogeneous microstructures consisting of a homogeneous matrix material with initially 12% and 30% volume fractions of voids are studied. To generate a random distribution of cavities in the matrix with a prescribed volume fraction, maximum diameter of holes and minimum distance between two neighbouring holes, for a two-dimensional RVE, the procedure from Hall (1991) and Smit (1998) has been adopted. The microstructural cells used in the calculations are presented in figure 7. It is worth mentioning that the absolute size of the microstructure is irrelevant for the first-order computational homogenization analysis (see also discussion in section 8).

The matrix material behaviour has been described by a modified elasto-visco-plastic Bodner-Partom model van der Aa et al. (2000). This choice is motivated by the intention to demonstrate that the method is well-suited for complex microstructural material behaviour, e.g. non-linear history and strain rate dependent at large strains. The material parameters for annealed aluminum AA 1050 determined in van der Aa et al. (2000) have been used; elastic parameters: shear modulus $G = 2.6 \times 10^4$ MPa, bulk modulus $K =$

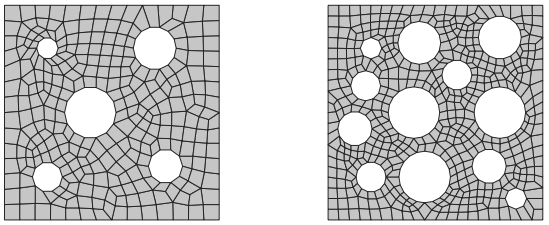

(a) (b)

Figure 7. Microstructural cells used in the calculations with 12% voids (a) and 30% voids (b).

7.8×10^4 MPa and viscosity parameters: $\Gamma_0 = 10^8\,\mathrm{s}^{-2}$, $m = 13.8$, $n = 3.4$, $Z_0 = 81.4$ MPa, $Z_1 = 170$ MPa.

Micro-macro calculations for the heterogeneous structure, represented by the RVEs shown in figure 7 have been carried out, simulating pure bending at a prescribed moment rate equal to $5 \times 10^5\,\mathrm{N\,m\,s}^{-1}$. Figure 8 shows the distribution plots of the effective plastic strain for the case of the RVE with 12% volume fraction voids at an applied moment equal to $6.8 \times 10^5\,\mathrm{N\,m}$ in the deformed macrostructure and in three deformed, initially identical RVEs at different locations in the macrostructure. Each hole acts as a plastic strain concentrator and causes higher strains in the RVE than those occurring in the homogenized macrostructure. In the present calculations the maximum effective plastic strain in the macrostructure is about 25%, whereas at RVE level this strain reaches 50%. It is obvious from the deformed geometry of the holes in figure 8 that the RVE in the upper part of the bended strip is subjected to tension and the RVE in the lower part to compression, while the RVE in the vicinity of the neutral axis is loaded considerably milder than the other RVEs. This confirms the conclusion that the method realistically describes the deformation modes of the microstructure.

In figure 9 the moment-curvature (curvature defined for the bottom edge of the specimen) diagram resulting from the computational homogenization approach is presented. To give an impression of the influence of the holes also the response of a homogeneous configuration (without cavities) is shown. It can be concluded that even the presence of 12% voids induces a reduction of the bending moment (at a certain curvature) of more than 25% in the plastic regime. This significant reduction in the bending moment may be attributed to the formation of microstructural shear bands, which are clearly observed in figure 8. This indicates that in order to capture such an effect a detailed microstructural analysis is required. A straightforward

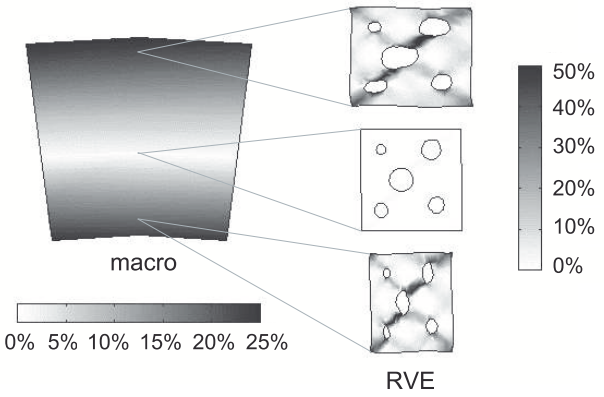

Figure 8. Distribution of the effective plastic strain in the deformed macrostructure and in three deformed RVEs, corresponding to different points of the macrostructure.

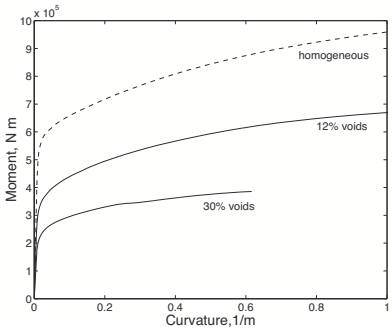

Figure 9. Moment-curvature diagram resulting from the first-order computational homogenization analysis.

application of, for example, the rule of mixtures would lead to erroneous results.

7 The RVE in first-order computational homogenization

7.1 General concept of an RVE

The computational homogenization approach, as well as most of other homogenization techniques, are based on the concept of a representative volume element (RVE). An RVE is a model of a material microstructure to be used to obtain the response of the corresponding homogenized macroscopic continuum in a macroscopic material point. Thus, the proper choice of the RVE largely determines the accuracy of the modelling of a heterogeneous material.

There appear to be two significantly different ways to define a representative volume element Drugan and Willis (1996). The first definition requires an RVE to be a statistically representative sample of the microstructure, i.e. to include virtually a sampling of all possible microstructural configurations that occur in the composite. Clearly, in the case of a non-regular and non-uniform microstructure such a definition leads to a considerably large RVE. Therefore, RVEs that rigorously satisfy this definition are rarely used in actual homogenization analyses. This concept is usually employed when a computer model of the microstructure is being constructed based on experimentally obtained statistical information (see e.g. Shan and Gokhale (2002)).

Another definition characterizes an RVE as the smallest microstructural volume that sufficiently accurately represents the overall macroscopic properties of interest. This usually leads to much smaller RVE sizes than the statistical definition described above. However, in this case the minimum required RVE size also depends on the type of material behaviour (e.g. for elastic behaviour usually much smaller RVEs suffice than for plastic behaviour), macroscopic loading path and difference of properties between heterogeneities. Moreover, the minimum RVE size, that results in a good approximation of the overall material properties, does not always lead to adequate distributions of the microfields within the RVE. This may be important if, for example, microstructural damage initiation or evolving microstructures are of interest.

The latter definition of an RVE is closely related to the one established by Hill Hill (1963), who argued that an RVE is well-defined if it reflects the material microstructure and if the responses under uniform displacement and traction boundary conditions coincide. If a microstructural cell does not contain sufficient microstructural information, its overall responses under uniform displacement and traction boundary conditions will differ. The homogenized properties determined in this way are called “apparent”, a no-

tion introduced by Huet Huet (1990). The apparent properties obtained by application of uniform displacement boundary conditions on a microstructural cell usually overestimate the real effective properties, while the uniform traction boundary conditions lead to underestimation. As has been verified by a number of authors van der Sluis et al. (2000); Terada et al. (2000), for a given microstructural cell size, the periodic boundary conditions provide a better estimation of the overall properties, than the uniform displacement and uniform traction boundary conditions. This conclusion also holds if the microstructure does not really possess geometrical periodicity Terada et al. (2000). Increasing the size of the microstructural cell leads to a better estimation of the overall properties, and, finally, to a "convergence" of the results obtained with the different boundary conditions to the real effective properties of the composite material, as schematically illustrated in figure 10. The convergence of the apparent properties towards the effective ones at increasing size of the microstructural cell has been investigated in Huet (1990, 1999); Ostoja-Starzewski (1998, 1999); Pecullan et al. (1999); Terada et al. (2000).

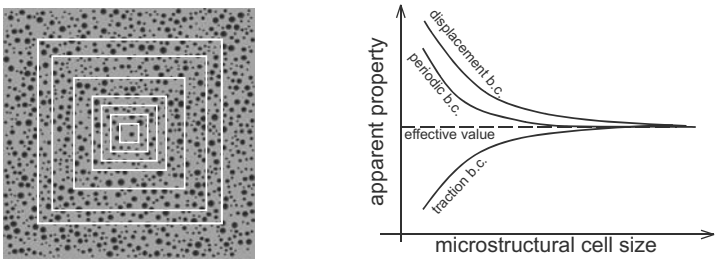

(a) (b)

Figure 10. (a) Several microstructural cells of different sizes. (b) Convergence of the apparent properties to the effective values with increasing microstructural cell size for different types of boundary conditions.

7.2 Unit cells versus RVEs

In practice, instead of a representative volume element, a unit cell is often used as a microstructural model, since it requires substantially less computational effort. This section examines the possible error, which is made in the obtained overall response of a multi-phase material, if the analysis is performed on a unit cell instead of an RVE.

As the simplest unit cell, a piece (for example a square or cube) of the matrix material containing a single heterogeneity (e.g. inclusion or void)

could be suggested. The use of such a unit cell implicitly assumes a regular arrangement of the heterogeneities in the matrix, which contradicts the observations that almost all materials have a non-periodic or even spatially random microstructural composition. Examples are precipitates in metal alloys arranged randomly by their nature and artificial fiber reinforced composites, possessing a non-regular distribution of the fibers due to the production process. At the same time, several experimental evidences exist showing that the spatial variability in the microstructure significantly influences the overall behaviour and particularly the fracture characteristics of composites, as reported in Mackay (1990); Barsoum et al. (1992).

Different authors, e.g. Brockenbrough et al. (1991); Nakamura and Suresh (1993); Ghosh et al. (1996); Moulinec and Suquet (1998), have performed a comparison of the overall composite responses resulting from the modelling of regular and random structures. They have found a significant response difference in the plastic regime, while there is almost no deviation in elastic regime. Also it has been shown Smit et al. (1999), that softening behaviour of a regularly composed structure may change to hardening in the case of a random composition. Most of these considerations, except for the latter, have been performed for small deformations, very simple elasto-plastic behaviour and relatively stiff inclusions (fibers). In this section the overall behaviour of regular and random structures is compared at large deformations, non-linear history dependent material behaviour, for voided material (an appropriate approximation for material with soft inclusions). Apart from the calculations on the microstructural cell (tensile configuration), also a full multi-scale analysis (pure bending) of both regular and random structures is presented.

A material with a 12% volume fraction of voids is considered. The regularly stacked structure is modelled by a square unit cell containing a single hole (figure 11a). For the modelling of a random structure 10 different unit cells with non-regular arrangements of voids with a distribution of void sizes have been generated (figure 11b). The averaged behaviour of these 10 unit cells is expected to be representative for the real random structure with a given volume fraction of heterogeneities. Using several small non-regular unit cells instead of one larger RVE also allows to estimate the amount of deviation of the apparent properties obtained by the unit cell modelling, from the effective values for different types of material models and loading histories.

In the subsequent sections a comparison is performed for three different constitutive models of the matrix material: hyper-elastic, elasto-visco-plastic with hardening and elasto-visco-plastic with intrinsic softening. First uniaxial extension (under plane strain conditions) of a macroscopic sample

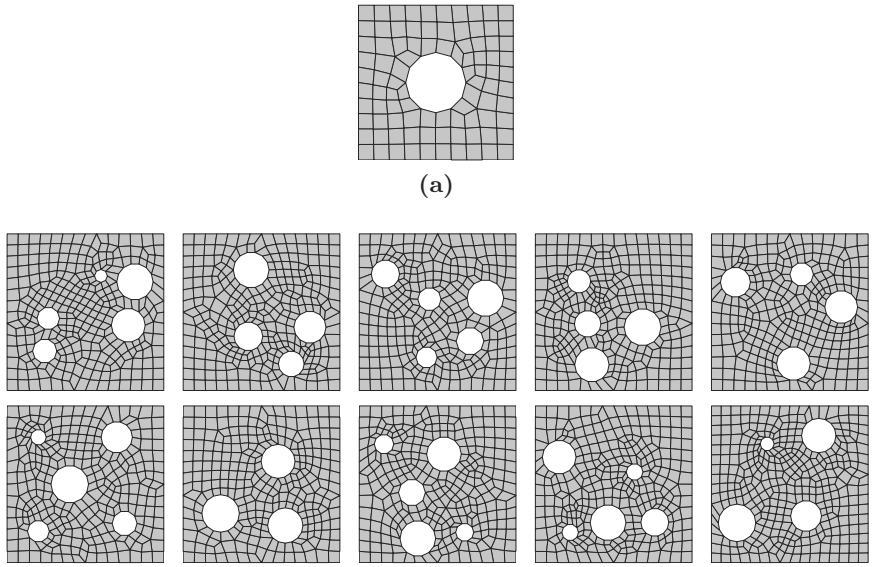

Figure 11. Unit cell with one hole (a), representing a regular structure, and 10 randomly composed unit cells (b).

is considered. Because in this case the macroscopic deformation field is homogeneous a full micro-macro modelling is not necessary and an analysis of an isolated unit cell with adequate boundary conditions (periodic) suffices. In the last section the results of a micro-macro simulation of bending using random and regular microstructures are compared.

Elastic behaviour, tension First, a comparison of the overall behaviour of regular and random structures is carried out for the case of hyperelastic behaviour of the matrix material, modelled as a compressible Neo-Hookean material. The material parameters used in the calculations are $K = 2667\,\mathrm{MPa}$, $G = 889\,\mathrm{MPa}$.

Figure 12 shows the stress-strain curves for the unit cells with regular and random void stacking. For small deformations there is almost no difference in the responses originating from the regular and random void distributions. This result is in agreement with the experiences reported in the literature for small deformations, see, e.g. Brockenbrough et al. (1991);

Nakamura and Suresh (1993); Moulinec and Suquet (1998). For large deformations the stiffer behaviour of the regular structure becomes a little bit more pronounced, however, the deviations remain small. The difference between the response of the regular structure and the response averaged over the random unit cells does not exceed 2%. This small deviation is explained by figure 13, presenting the distribution of the equivalent von Mises stress in the regular unit cell and in a random unit cell for 20% macroscopic strain. The stress field around any hole of the random structure is almost the same as around the hole of the regular structure, which indicates little interaction between voids. If only the averaged elastic constants are of interest, it is concluded that calculations performed on the simplest regular unit cell usually provide an answer within an acceptable tolerance.

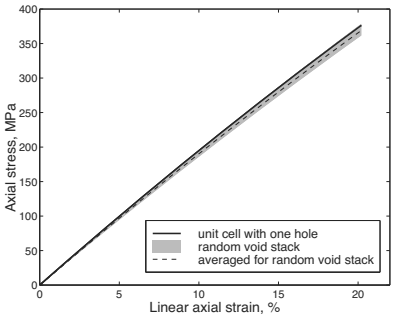

Figure 12. Tensile stress-strain responses (unit cell averages) of the regular and random structures in a voided hyper-elastic matrix material.

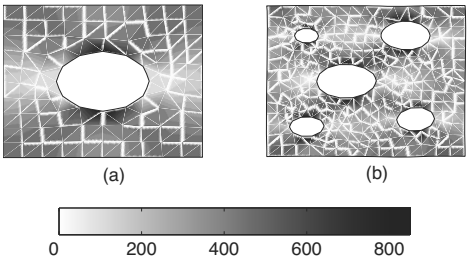

Figure 13. Distribution of the equivalent von Mises stress (MPa) in the deformed regular (a) and random (b) structures in a voided hyper-elastic matrix material.

Elasto-visco-plastic behaviour with hardening, tension The influence of the randomness of the microstructure on the macroscopic response becomes more significant when plastic yielding of one or more constituents occurs. This section investigates the responses of the regular and random unit cells under tensile loading when the matrix material exhibits elasto-visco-plastic behaviour with hardening. The constitutive description is given by the Bodner-Partom model van der Aa et al. (2000). The material parameters are the same as those used in section 6. The unit cells are subjected to uniaxial tension at a constant strain rate of $0.5\,\mathrm{s}^{-1}$.

In figure 14 the stress-strain curves are presented. In this case the difference between the overall response of the regular structure and the averaged response of the random structures reaches 10%. The rather large scattering in the responses of different random cells is due to the small number of voids included. As has been demonstrated in Smit (1998), the scattering is significantly reduced if microstructural cells contain more heterogeneities. The averaged response is, however, hardly affected, provided that a sufficient number of random realizations has been considered.

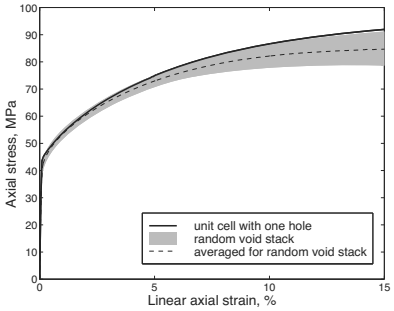

Figure 14. Tensile stress-strain responses (unit cell averages) of the regular and random structures for an elasto-visco-plastic matrix material with hardening.

The fundamental mechanism that governs the difference between the response of the regular structure and the averaged response of the random structures is illustrated in figure 15, where the distribution of the effective plastic strain in the deformed regular and random unit cells at 15% applied macroscopic strain is presented. In the regular unit cell the ligaments yield simultaneously rather than sequentially with increasing macroscopic strain, which is the case for the random unit cell. As a result, at the same value of the macroscopic strain the regular unit cell is deformed relatively smoothly,

while some ligaments in the random unit cell have already accumulated a significant amount of plastic strain. Consequently, the regular unit cell (in fact a structure with a periodic stacking of heterogeneities) has a larger overall stiffness than a random configuration.

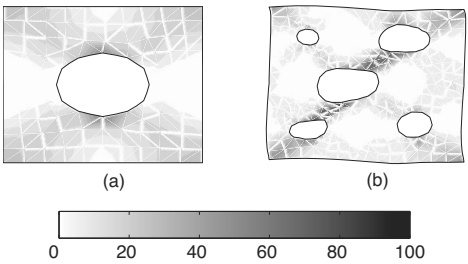

Figure 15. Distribution of the effective plastic strain in the deformed regular (a) and random (b) structures for an elasto-visco-plastic matrix material with hardening.

Elasto-visco-plastic behaviour with softening, tension The difference in yielding mechanisms for regular and random microstructures outlined in the previous section causes not only a quantitative deviation in the responses of these structures (as illustrated by figure 14), but in some cases also the qualitative character changes, as has been shown in Smit et al. (1999). For example, such a phenomenon can be observed when the matrix material is described by a generalized compressible Leonov model with intrinsic softening and subsequent hardening. The model is designed for the plastic deformation of polymers and incorporates a stress dependent Eyring viscosity extended by pressure dependence and intrinsic softening effects. Details of this model can be found in Baaijens (1991); Tervoort (1996); Govaert et al. (2000).

The resulting stress-strain curves for uniaxial tension of polycarbonate at a constant strain rate of $0.01\,\mathrm{s}^{-1}$ are given in figure 16. The overall behaviour of the regular structure in the plastic regime exhibits some initial softening followed by hardening. The response of the regular structure is, in fact, similar to the response of one single ligament, that softens according to the intrinsic material behaviour. A completely different response can be observed for the random configurations. Although some of the random unit cells also demonstrate some softening behaviour, originating from the relatively simple composition of the unit cells used in the calculations, the average response of the random unit cells does not show any softening but

exhibits continuous hardening. This is caused by the sequential appearance of elastic, softening and hardening zones within the random microstructure.

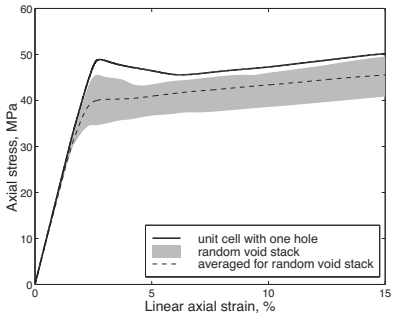

Figure 16. Tensile stress-strain responses (RVE averages) of the regular and random structures for an elasto-visco-plastic matrix material with intrinsic softening and subsequent hardening.

This example illustrates that the overall response of heterogeneous materials, when detersi3joda!mined from a modelling by a regular structure, should be interpreted with great care, particularly in the case of complex material behaviour (e.g. in case of softening followed by hardening or vice versa).

Elasto-visco-plastic behaviour with hardening, bending The comparison of the overall behaviour of the regular and random microstructures performed above has been based on the averaged behaviour of a single unit cell subjected to a particular loading history (uniaxial tension). The question remains how the randomness of the microstructure does influence the overall behaviour when a macroscopic sample is deformed heterogeneously, so that potentially every material point of the sample is subjected to a different loading history. In order to investigate this item the computational homogenization approach is a helpful tool.

As an example the influence of the spatial composition of the microstructure on the overall moment-curvature response of the voided material under pure bending is studied. The behaviour of the matrix material is described by the Bodner-Partom elasto-visco-plastic model with hardening. The macrogeometry and the material parameters are the same as these used in section 6.

Figure 17 shows the moment-curvature diagram resulting from the full

micro-macro analysis of pure bending of the material using the regular and the random microstructures. Again, the regular structure exhibits a stiffer response than the averaged random result, while the maximum deviation is only about 5%, which is considerably less than for the tensile test with the same material behaviour (figure 14). This smaller deviation originates from the fact that in case of bending all the unit cells assigned to the various macroscopic points over the height of the bended strip are loaded differently, see figure 8. The unit cell at the top of the bended strip experiences tension, so that the observations dealt with in the previous examples apply. At the same time, there are also unit cells that are stretched less or still are in elastic regime, like for example the one in the vicinity of the neutral line, so that in average for the whole bending process the influence of randomness can be expected to be smaller than for uniaxial extension.

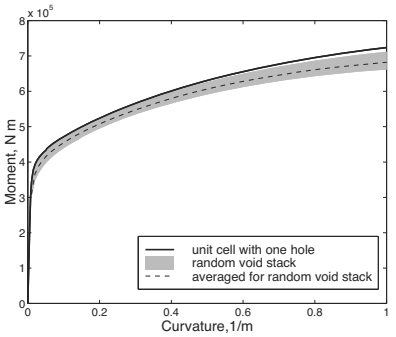

Figure 17. Moment-curvature responses of the regular and random structures for an elasto-visco-plastic matrix material with hardening.

8 Second-order computational homogenization

In spite of the attractive characteristics listed above, there are a few important limitations of the first-order framework, which can be summarized as follows

- The principle of separation of scales must be respected. Hence, the characteristic length that characterizes the spatial variations of the macroscopic loading must be very large with respect to the size of the microstructure. As a consequence, only simple first-order deformation modes (tension, compression, shear or combinations thereof) of the microstructure can be retrieved. The case shown in figure 8, which is

a typical bending mode, which from a physical point of view should appear for small, but finite, microstructural cells, cannot be found.
- The framework is completely insensitive to the absolute size of the microstructural constituents (scale independent). Size effects emanating from the absolute size at the micro scale cannot be dealt with properly.
- Macroscopic gradients must remain very small with respect to the micro scale. Localization problems, where non-uniform macroscopic deformations arise, cannot be solved properly.

Whenever strong gradients appear at the macro-level (localization, size effects) care must be taken in using a first-order scheme. In all other cases, one should continue using it and not jump to a second-order scheme for which an additional price in complexity and computational costs is to be paid.

In order to overcome these shortcomings, the computational homogenization methodology has been extended recently to higher-order continua (Geers et al., 2001; Kouznetsova et al., 2002; Kouznetsova, 2002; Geers et al., 2003; Kouznetsova et al., 2004b,a). In this course, the methodology and the essential parts of the multi-scale kinematics and statics will be outlined briefly, whereas more details can be found in the cited references. The method is next applied to heterogeneous multi-phase microstructures, as typically the case in most metals, polymer blends and composites. Some comments on the parallel implementation of the multi-scale technique are given and an illustrative example is used to scrutinize the added value of the second-order framework in relation to the more standard first-order scheme.

8.1 Principles

The second-order case, which may be considered as a generalization of the classical first-order scheme, departs from a Taylor series expansion of the classical nonlinear deformation map, $\vec{x} = \phi(\vec{X})$, applied to a finite material vector $\Delta\vec{x}$ in the deformed state:

$$\Delta\vec{x} \;=\; \mathbf{F}_{\mathrm{M}}{\cdot}\Delta\vec{X} + \tfrac{1}{2}\Delta\vec{X}{\cdot}{}^{3}\mathbf{G}_{\mathrm{M}}{\cdot}\Delta\vec{X} + \mathcal{O}\left(\Delta\vec{X}^{3}\right) \tag{71}$$

Using this Taylor series expansion, the macroscopic (coarse scale) kinematics is determined through the deformation gradient tensor $\mathbf{F}_{\mathrm{M}}$ and its Lagrangian gradient ${}^{3}\mathbf{G}_{\mathrm{M}} = \vec{\nabla}_{0,\mathrm{M}}\mathbf{F}_{\mathrm{M}}$. The key point in the second-order two-scale framework, resides in applying relation (71) to a representative part of the microstructure, such that a classical boundary value problem is obtained at the micro scale (or fine scale). The scale bridging is then realized through the application of averaging theorems. This is schematically depicted in figure 18. Note that the tensor ${}^{3}\mathbf{G}_{\mathrm{M}}$ has a minor symmetry,

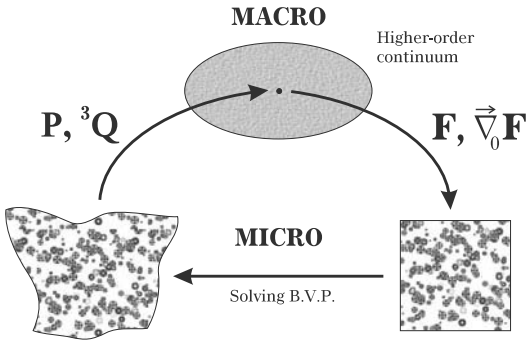

Figure 18. Second-order computational homogenization

${}^3\mathbf{G}_{\rm M} = {}^3\mathbf{G}_{\rm M}^T$ (or $G_{Mijk} = G_{Mkji}$ in index notation), which is used throughout this chapter.

8.2 Two-scale higher-order kinematics

In order to apply equation (71) to the fine scale, all higher-order terms (represented by $\mathcal{O}(\Delta\vec{X}^3)$) are condensed into an unknown microfluctuation field $\vec{w}$, which represents the fine scale contribution in the kinematics. Hence,

$$\Delta\vec{x} \;=\; \mathbf{F}_{\rm M}{\cdot}\Delta\vec{X} + \tfrac{1}{2}\Delta\vec{X}{\cdot}{}^3\mathbf{G}_{\rm M}{\cdot}\Delta\vec{X} + \vec{w} \tag{72}$$

Applying this to an undeformed volume V_0 (the RVE) with a geometrical center $\vec{X}_c$ that is located in $\vec{x}_c$ after deformation gives (notice the similarity and differences with the elaboration in the previous section, equation (5)).

$$\vec{x} - \vec{x}_c \;=\; \mathbf{F}_{\rm M}{\cdot}(\vec{X} - \vec{X}_c) + \tfrac{1}{2}(\vec{X} - \vec{X}_c){\cdot}{}^3\mathbf{G}_{\rm M}{\cdot}(\vec{X} - \vec{X}_c) + \vec{w} \tag{73}$$

Eliminating rigid body displacements like for the first-order case (e.g. by fixing a boundary point 1) then leads to

$$\vec{x} \;=\; \vec{c} + \mathbf{F}_{\rm M}{\cdot}(\vec{X} - \vec{X}_c) + \tfrac{1}{2}(\vec{X} - \vec{X}_c){\cdot}{}^3\mathbf{G}_{\rm M}{\cdot}(\vec{X} - \vec{X}_c) + (\vec{w} - \vec{w}_1) \tag{74}$$

with

$$\vec{c} \;= \vec{X}_1 + \mathbf{F}_{\rm M}{\cdot}(\vec{X}_1 - \vec{X}_c) + \tfrac{1}{2}(\vec{X}_1 - \vec{X}_c){\cdot}{}^3\mathbf{G}_{\rm M}{\cdot}(\vec{X}_1 - \vec{X}_c) \tag{75}$$

$$\vec{x}_c \;= \vec{c} - \vec{w}_1 \tag{76}$$

The microscopic deformation gradient tensor $\mathbf{F}_{\rm m}$ is easily reconstructed as

$$\begin{aligned} \mathbf{F}_{\rm m} \;&= (\vec{\nabla}_{0,{\rm m}}\vec{x})^T \\ &= \mathbf{F}_{\rm M} + (\vec{X} - \vec{X}_c){\cdot}{}^3\mathbf{G}_{\rm M} + (\vec{\nabla}_{0,{\rm m}}(\vec{w} - \vec{w}_1))^T \end{aligned} \tag{77}$$

Applying the earlier introduced scale transition relation (13) with respect to equation (77) then leads to two kinematical constraints (to be imposed on the RVE)

$$\frac{1}{V_0}\int_{V_0}(\vec{X}-\vec{X}_c)dV_0 \;=\; \vec{0} \tag{78}$$

$$\frac{1}{V_0}\int_{V_0}(\vec{\nabla}_{0,\mathrm{m}}(\vec{w}-\vec{w}_1))^T\,dV_0 \;=\; \frac{1}{V_0}\int_{\Gamma_0}(\vec{w}-\vec{w}_1)\vec{N}\,d\Gamma_0 = \mathbf{0} \tag{79}$$

where the divergence theorem was used to derive the latter relation. Equation (78) is clearly satisfied here, since the Taylor series has been expanded with respect to the geometrical centre $\vec{X}_c$ in equation (73). This appears to be a necessary condition in the second-order case, which deviates from the first-order scheme where any point to develop (4) around (instead of $\vec{X}_c$) gives the same result. The second constraint (79) applies to the unknown fluctuation field. Logically, the integral involves $(\vec{w}-\vec{w}_1)$, which implies a constraint on the boundary position vectors $\vec{x}$ through (74). There are various ways to make this boundary integral zero, e.g. by constraining $(\vec{w}-\vec{w}_1)=\vec{0}$ for all points of the RVE (Taylor/Voigt), or by constraining $(\vec{w}-\vec{w}_1)=\vec{0}$ at the boundary of the RVE only (displacement or kinematic boundary condition), or through the application of periodic boundary conditions on the microfluctuation field (the macroscopic field is generally not periodic in the second-order case!). The latter conditions are used here, leading to the following microperiodicity equations valid between the left(L)-right(R) and bottom(B)-top(T) boundaries of a two-dimensional rectangular RVE as shown in figure 19.

$$\vec{w}_L \;=\; \vec{w}_R \qquad\qquad \vec{w}_B \;=\; \vec{w}_T \tag{80}$$

Note that again all equations involve the microfluctuation field with respect to $\vec{w}_1$. Any choice for $\vec{w}_1$ will then lead to the same solution (except for $\vec{x}_c$). This is also obvious from the constraint relation (79), which can be easily elaborated to a format in which the contribution of $\vec{w}_1$ vanishes, i.e.

$$\int_{\Gamma_0}(\vec{w}-\vec{w}_1)\vec{N}\,d\Gamma_0 \;=\; \int_{\Gamma_0}\vec{w}\vec{N}\,d\Gamma_0 \;=\; \mathbf{0} \tag{81}$$

It is easy to show that the micro scale problem defined by the equations (72), (78), (80), applied to the rectangular 2D RVE depicted in figure 19 with periodic microfluctuations, fully determines the kinematics of the four corner points (Geers et al., 2001; Kouznetsova et al., 2002). This

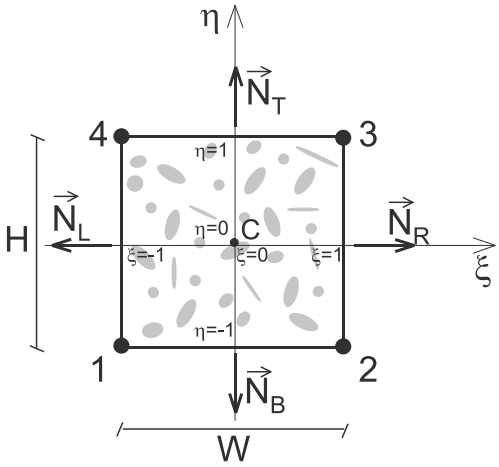

Figure 19. Lagrangian undeformed 2D reference RVE

set of equations imposes 8 macroscopic degrees-of-freedom to the 2D microstructure, whereas the full macroscopic kinematics consists of 12 degrees-of-freedom (2 rigid body displacement, 4 degrees-of-freedom in $\mathbf{F}_{\mathrm{M}}$ and 6 degrees-of-freedom in the minor-symmetric ${}^{3}\mathbf{G}_{\mathrm{M}}$). The missing kinematical quantities appear to be the stretch gradients (Geers et al., 2001; Kouznetsova et al., 2002), i.e. so far an RVE with 8 macroscopic degrees-of-freedom has been established, where the displacements are prescribed through the four corner nodes. This is a typical example of couple stress homogenization.

In order to incorporate the entire gradient field, the set of averaging relations needs to be completed in order to account for the missing stretch gradient degrees-of-freedom of ${}^{3}\mathbf{G}_{\mathrm{M}}$. On the basis of the Taylor series expansion (72), it is easy to show that the following averaging theorem can be derived (by means of some manipulations of the equations given in Kouznetsova et al. (2002)), relating ${}^{3}\mathbf{G}_{\mathrm{M}}$ to the position vectors $\vec{x}$ (implicitly incorporating the fine scale contribution through (74)) of all material

points in the the square RVE with initial size W and volume V_0:

$$\frac{W^2}{12}\left[{}^3\mathbf{G}_{\mathrm{M}} + \tfrac{1}{2}\left(\mathbf{II} : {}^3\mathbf{G}_{\mathrm{M}}^{RT}\right)^{RT}\right] + (\mathbf{I}\vec{c})^{RT} = \frac{1}{2V_0}\int_{V_0}\left(\vec{\nabla}_{0,\mathrm{m}}(\vec{x}\vec{X}) + [\vec{\nabla}_{0,\mathrm{m}}(\vec{x}\vec{X})]^T\right)dV_0 \quad (82)$$

In here, $\mathbf{I}$ is the second-order unit tensor, and ^{RT} stands for the right transpose, i.e. $T_{ijk}^{RT} = T_{ikj}$ in index notation. The third term in the left-hand side of this equation is present to account for the deformed position $\vec{x}_c$ of the center of the undeformed RVE, which is generally no longer the center of the deformed RVE. Computing the integral in the right-hand side of the latter equation through substitution of equation (74), reveals

$$\frac{1}{2V_0}\int_{V_0}\left(\vec{\nabla}_{0,\mathrm{m}}(\vec{x}\vec{X}) + [\vec{\nabla}_{0,\mathrm{m}}(\vec{x}\vec{X})]^T\right)dV_0 = \frac{W^2}{12}{}^3\mathbf{G}_{\mathrm{M}} + \frac{W^2}{24}\left(\mathbf{II} : {}^3\mathbf{G}_{\mathrm{M}}^{RT}\right)^{RT} + [\mathbf{I}\vec{c}]^{RT} + \frac{1}{2V_0}\int_{\Gamma_0}\left(\vec{X}(\vec{w}-\vec{w}_1)\vec{N} + \vec{N}(\vec{w}-\vec{w}_1)\vec{X}\right)d\Gamma_0 \quad (83)$$

Enforcing the averaging relation (82) requires that the last integral in (83) should vanish, which leads to a new constraint on the microfluctuation field.

$$\int_{\Gamma_0}\left(\vec{X}(\vec{w}-\vec{w}_1)\vec{N} + \vec{N}(\vec{w}-\vec{w}_1)\vec{X}\right)d\Gamma_0 = {}^3\mathbf{0} \quad (84)$$

This boundary integral clearly incorporates $(\vec{w}-\vec{w}_1)$, which constrains the position vectors $\vec{x}$ of the boundary points through (74). The microfluctuation $\vec{w}_1$ (in the fixed boundary point) cannot be eliminated in general as done in the previously introduced boundary integral (81). If constraint (84) is enforced, it is easy to rewrite the averaging equation (82) as a boundary integral

$${}^3\mathbf{G}_{\mathrm{M}} + \tfrac{1}{2}\left(\mathbf{II} : {}^3\mathbf{G}_{\mathrm{M}}^{RT}\right)^{RT} + \frac{12}{W^2}[\mathbf{I}\vec{c}]^{RT} = \frac{6}{V_0 W^2}\int_{\Gamma_0}\left(\vec{X}\vec{x}\vec{N} + \vec{N}\vec{x}\vec{X}\right)d\Gamma_0 \quad (85)$$

Equation (85) typically illustrates that $^3\mathbf{G}_{\mathrm{M}}$ is imposed on the RVE boundary, which is necessary to construct a classical boundary value problem at the micro scale.

For an initially square RVE ($H = W$ in figure 19), on which the microperiodicity equations (80) for the microfluctuation field hold, the constraint (84) can be simplified to

$$\begin{aligned} \int_{\Gamma_{0L}} (\vec{w}_L - \vec{w}_1) d\Gamma_0 &= \vec{0} \\ \int_{\Gamma_{0B}} (\vec{w}_B - \vec{w}_1) d\Gamma_0 &= \vec{0} \end{aligned} \tag{86}$$

Clearly, these two conditions enforce the shape of a part of the boundary to be equal in average to the shape ensuing from the macroscopic field. Prescribing (86) at the boundaries can be done by generalized displacement constraints (non-homogeneous tying relations), see (Kouznetsova et al., 2002; Kouznetsova, 2002) for more details on this topic. Again, it is obvious that imposing $\vec{w}_1 = \vec{0}$ does not influence the solution for the two-scale homogenization.

Note that the macroscopic ${}^3\mathbf{G}_{\mathrm{M}}$ is not the volume average of the microscopic ${}^3\mathbf{G}_{\mathrm{m}} = \vec{\nabla}_{0,\mathrm{m}}\mathbf{F}_{\mathrm{m}}$. This not possible if one wants to construct a classical boundary value problem at the micro scale. The scale transition is here driven by boundary integrals involving displacements of boundary points of the RVE only. Enforcing ${}^3\mathbf{G}_{\mathrm{M}}$ to be the volume average of ${}^3\mathbf{G}_{\mathrm{m}}$ would lead to higher-order boundary conditions on the microstructural fluctuation field, which would make the fine scale problem second-order as well.

8.3 Extracting stress tensors

The macroscopic stress quantities are next extracted from the analysis of the deformed RVE by equating the macroscopic work per unit of volume to the average work performed on the RVE (Hill-Mandel or macrohomogeneity condition). For the second-order case, this condition reads

$$\frac{1}{V_0}\int_{V_0} \mathbf{P}_{\mathrm{m}} : \delta\mathbf{F}_{\mathrm{m}}^T dV_0 \; = \mathbf{P}_{\mathrm{M}} : \delta\mathbf{F}_{\mathrm{M}}^T + {}^3\mathbf{Q}_{\mathrm{M}} \vdots \delta{}^3\mathbf{G}_{\mathrm{M}} \tag{87}$$

In here, $\mathbf{P}_{\mathrm{M}}$ is the macroscopic first Piola-Kirchhoff stress tensor, $\mathbf{P}_{\mathrm{m}}$ its microstructural counterpart and ${}^3\mathbf{Q}_{\mathrm{M}}$ the higher-order stress tensor which is work-conjugated to ${}^3\mathbf{G}_{\mathrm{M}}$. Note that equation (87) in fact defines the two macroscopic stress tensors $\mathbf{P}_{\mathrm{M}}$ and ${}^3\mathbf{Q}_{\mathrm{M}}$.

The microstructural work (per unit of volume in the reference state) can

be written as

$$\delta W_{0\mathrm{M}} = \frac{1}{V_0}\int\limits_{V_0} \mathbf{P}_{\mathrm{m}} : \delta\mathbf{F}^{c}_{\mathrm{m}}\mathrm{d}V_0 = \frac{1}{V_0}\int\limits_{\Gamma_0} \vec{p}\cdot\delta\Delta\vec{x}\ \mathrm{d}\Gamma_0, \tag{88}$$

where use has been made of the divergence theorem and the static equilibrium equation in the microstructure (2). Taking the variation of the position vector $\delta\Delta\vec{x}$ according to (72) leads to

$$\delta\Delta\vec{x} = \delta\mathbf{F}_{\mathrm{M}}\cdot\vec{X} + \tfrac{1}{2}\vec{X}\cdot\delta^3\mathbf{G}_{\mathrm{M}}\cdot\vec{X} + \delta\Delta\vec{w}, \tag{89}$$

which after substitution in equation (88) yields

$$\delta W_{0\mathrm{M}} = \frac{1}{V_0}\int\limits_{\Gamma_0} \vec{p}\vec{X}\ \mathrm{d}\Gamma_0 : \delta\mathbf{F}^{c}_{\mathrm{M}} + \frac{1}{2V_0}\int\limits_{\Gamma_0} \vec{X}\vec{p}\vec{X}\ \mathrm{d}\Gamma_0\ \vdots\ \delta^3\mathbf{G}_{\mathrm{M}} + \frac{1}{V_0}\int\limits_{\Gamma_0} \vec{p}\cdot\delta\Delta\vec{w}\ \mathrm{d}\Gamma_0. \tag{90}$$

Since the boundary constraints (80) do not contribute to the total work and accounting for (86), the last term in (90) can be proven to disappear

$$\int\limits_{\Gamma_0} \vec{p}\cdot\delta\Delta\vec{w}\ \mathrm{d}\Gamma_0 = 0, \tag{91}$$

manifesting the fact that the microstructural fluctuation field does not affect the average variation of the microscopic work.

Elaboration of this equation leads to two boundary integrals that permit to compute the stress tensors $\mathbf{P}_{\mathrm{M}}$ and ${}^3\mathbf{Q}_{\mathrm{M}}$:

$$\mathbf{P}_{\mathrm{M}} = \frac{1}{V_0}\int\limits_{\Gamma_0} \vec{p}\vec{X}\ d\Gamma_0 \tag{92}$$

$${}^3\mathbf{Q}_{\mathrm{M}} = \frac{1}{2V_0}\int\limits_{\Gamma_0} \vec{X}\vec{p}\vec{X}\ \mathrm{d}\Gamma_0 \tag{93}$$

Both stress tensors can be easily computed once the boundary value problem on the micro scale has been solved.

The above formulas relate the macroscopic stress tensor and the macroscopic higher-order stress tensor to microstructural variables defined on the RVE boundary. The relations (92) and (93) can also be transformed into volume integrals, allowing the macroscopic stress measures to be expressed in terms of volume averages of microstructural quantities. The macroscopic

stress tensor $\mathbf{P}_{\mathrm{M}}$ again equals the volume average of the microscopic stress tensor $\mathbf{P}_{\mathrm{m}}$

$$\mathbf{P}_{\mathrm{M}} = \frac{1}{V_0}\int_{V_0} \mathbf{P}_{\mathrm{m}} dV_0 \tag{94}$$

The proof of this equation is identical to that for the first-order framework (for the derivation see (32)-(33)).

The derivation for the higher-order stress tensor ${}^3\mathbf{Q}_{\mathrm{M}}$ follows the same procedure. Applying the divergence theorem to transform the boundary integral in (93) to a volume integral gives

$$\begin{aligned} {}^3\mathbf{Q}_{\mathrm{M}} &= \frac{1}{2V_0}\int_{\Gamma_0} \vec{X}\vec{p}\vec{X}\mathrm{d}\Gamma_0 = \frac{1}{2V_0}\int_{\Gamma_0} ((\vec{N}\cdot\mathbf{P}^c_{\mathrm{m}})\vec{X}\vec{X})^{LC}\mathrm{d}\Gamma_0 \\ &= \frac{1}{2V_0}\int_{V_0} (\nabla_{0\mathrm{m}}\cdot(\mathbf{P}^c_{\mathrm{m}}\vec{X}\vec{X}))^{LC}\mathrm{d}V_0, \end{aligned} \tag{95}$$

where the superscript LC denotes left conjugation, $T^{LC}_{ijk} = T_{jik}$. Finally using the equality

$$\begin{aligned} \nabla_{0\mathrm{m}}\cdot(\mathbf{P}^c_{\mathrm{m}}\vec{X}\vec{X}) &= (\nabla_{0\mathrm{m}}\cdot\mathbf{P}^c_{\mathrm{m}})\vec{X}\vec{X} + \mathbf{P}_{\mathrm{m}}\cdot(\nabla_{0\mathrm{m}}\vec{X})\vec{X} + (\vec{X}\mathbf{P}_{\mathrm{m}}\cdot(\nabla_{0\mathrm{m}}\vec{X}))^{LC} \\ &= \mathbf{P}_{\mathrm{m}}\vec{X} + (\vec{X}\mathbf{P}_{\mathrm{m}})^{LC}, \end{aligned} \tag{96}$$

where equilibrium has been exploited, the relation between the macroscopic higher-order stress tensor and microstructural quantities is obtained

$${}^3\mathbf{Q}_{\mathrm{M}} = \frac{1}{2V_0}\int_{V_0} \left(\mathbf{P}^T_{\mathrm{m}}\vec{X} + \vec{X}\mathbf{P}_{\mathrm{m}}\right) dV_0 \tag{97}$$

Note that the macroscopic higher-order stress tensor ${}^3\mathbf{Q}_{\mathrm{M}}$ does not equal the volume average of its microscopic counterpart $\vec{\nabla}_{0,\mathrm{m}}\mathbf{P}_{\mathrm{m}}$. Like for ${}^3\mathbf{G}_{\mathrm{M}}$ this is due to the fact that the micro scale problem is formulated as a classical boundary value problem. It is clear from (97) that ${}^3\mathbf{Q}_{\mathrm{M}}$ can be interpreted as the first moment (with respect to the RVE center) of the microscopic first Piola-Kirchhoff stress tensor $\mathbf{P}_{\mathrm{m}}$ over the initial RVE volume V_0.

8.4 Two-scale computational solution strategy

The boundary constraints (86) can be explicitly written in terms of the displacement vectors of the boundary points in the form

$$\int_{\Gamma_{0\mathrm{L}}} \vec{u}_{\mathrm{L}}\ \mathrm{d}\Gamma_0 = \vec{u}_{L^*}(\mathbf{F}_{\mathrm{M}}, {}^3\mathbf{G}_{\mathrm{M}}), \qquad \int_{\Gamma_{0\mathrm{B}}} \vec{u}_{\mathrm{B}}\ \mathrm{d}\Gamma_0 = \vec{u}_{B^*}(\mathbf{F}_{\mathrm{M}}, {}^3\mathbf{G}_{\mathrm{M}}) \tag{98}$$

where $\vec{u}_{L^*}$ and $\vec{u}_{B^*}$ solely depend on the given $\mathbf{F}_\mathrm{M}$ and ${}^3\mathbf{G}_\mathrm{M}$ and RVE geometry as apparent from their definitions

$$\begin{aligned}\vec{u}_{L^*} =&(\mathbf{F}_\mathrm{M}-\mathbf{I})\cdot\int_{\Gamma_{0\mathrm{L}}}(\vec{X}_\mathrm{L}-\vec{X}_1)\,\mathrm{d}\Gamma_0+\tfrac{1}{2}{}^3\mathbf{G}_\mathrm{M}^{LC}:\int_{\Gamma_{0\mathrm{L}}}(\vec{X}_\mathrm{L}\vec{X}_\mathrm{L}-\vec{X}_1\vec{X}_1)\,\mathrm{d}\Gamma_0\\ \vec{u}_{B^*} =&(\mathbf{F}_\mathrm{M}-\mathbf{I})\cdot\int_{\Gamma_{0\mathrm{B}}}(\vec{X}_\mathrm{B}-\vec{X}_1)\,\mathrm{d}\Gamma_0+\tfrac{1}{2}{}^3\mathbf{G}_\mathrm{M}^{LC}:\int_{\Gamma_{0\mathrm{B}}}(\vec{X}_\mathrm{B}\vec{X}_\mathrm{B}-\vec{X}_1\vec{X}_1)\,\mathrm{d}\Gamma_0\end{aligned} \tag{99}$$

Once the BVP associated to the microstructural RVE problem is defined (boundary conditions, constitutive equations) the micro-problem can be solved with a standard finite element method. On the basis of the resulting boundary tractions, the RVE averaged stress tensors are extracted (see equations (94), (97))) and transported to the corresponding macroscopic material point.

For the finite element solution of the macroscopic problem a stiffness matrix at every macroscopic integration point is required. As emphasized earlier, in computational homogenization schemes there is no explicit form of the macroscopic constitutive behaviour assumed a priori. Like for the first-order case, the tangent operator is determined numerically by condensation of the microscopic stiffness matrix. For this, first the elaborated constraint relations between boundary nodes (equations (80), (86)) are applied to the total assembled stiffness matrix of the RVE following a similar procedure as presented for the first-order case. Details for the second-order case are given in Kouznetsova (2002); Kouznetsova et al. (2004b,a). This results in the elimination of the dependent degrees of freedom from the system of equations. The next step is to partition the remaining system of equations as

$$\begin{bmatrix}\underline{K}_{pp} & \underline{K}_{pf}\\ \underline{K}_{fp} & \underline{K}_{ff}\end{bmatrix}\begin{bmatrix}\delta\underset{\sim}{u}_p\\ \delta\underset{\sim}{u}_f\end{bmatrix}=\begin{bmatrix}\delta\underset{\sim}{f}_p\\ \underset{\sim}{0}\end{bmatrix} \tag{100}$$

where the subscript p refers to "prescribed" degrees of freedom (degrees of freedom through which the macroscopic tensors $\mathbf{F}_\mathrm{M}$ and ${}^3\mathbf{G}_\mathrm{M}$ are imposed on the RVE). In the present framework these are the degrees of freedom corresponding to the four corner nodes of the RVE ($\vec{u}_i, i=\overline{1,4}$) and to the degrees of freedom entering the RVE system of equations through the boundary constraints (98). The subscript f in (100) refers to all remaining "free" nodes. Elimination of $\delta\underline{u}_f$ from the system (100) then leads to the reduced stiffness matrix $\underline{K}_\mathrm{M}$ that relates the variations of the prescribed degrees of freedom to the variations of the associated forces

$$\underline{K}_\mathrm{M}\delta\underset{\sim}{u}_p=\delta\underset{\sim}{f}_p,\qquad\text{with}\quad\underline{K}_\mathrm{M}=\underline{K}_{pp}-\underline{K}_{pf}(\underline{K}_{ff})^{-1}\underline{K}_{fp} \tag{101}$$

The linearized constitutive relations for the second gradient continuum can be written as

$$\delta \mathbf{P}_{\mathrm{M}} = {}^{4}\mathbf{C}_{\mathrm{M}}^{(1)} : \delta \mathbf{F}_{\mathrm{M}}^{c} + {}^{5}\mathbf{C}_{\mathrm{M}}^{(2)} \vdots \delta^{3}\mathbf{G}_{\mathrm{M}}^{RC} \tag{102}$$

$$\delta^{3}\mathbf{Q}_{\mathrm{M}} = {}^{5}\mathbf{C}_{\mathrm{M}}^{(3)} : \delta \mathbf{F}_{\mathrm{M}}^{c} + {}^{6}\mathbf{C}_{\mathrm{M}}^{(4)} \vdots \delta^{3}\mathbf{G}_{\mathrm{M}}^{RC} \tag{103}$$

where the fourth-order tensor ${}^{4}\mathbf{C}_{\mathrm{M}}^{(1)}$, the fifth-order tensors ${}^{5}\mathbf{C}_{\mathrm{M}}^{(2)}$ and ${}^{5}\mathbf{C}_{\mathrm{M}}^{(3)}$ and the sixth-order tensor ${}^{6}\mathbf{C}_{\mathrm{M}}^{(4)}$ are the macroscopic consistent tangents. Using the RVE reduced stiffness matrix $\underline{\underline{K}}_{\mathrm{M}}$ rewritten in a tensor format such that

$$\sum_{j} \mathbf{K}_{\mathrm{M}}^{(ij)} \cdot \delta \vec{u}_{(j)} = \delta \vec{f}_{(i)}, \qquad i,j = 1,2,3,4,L^{*},B^{*} \tag{104}$$

permits to extract the macroscopic consistent tangents in the following format (see Kouznetsova et al. (2004a) for the derivation)

$$\begin{aligned}
{}^{4}\mathbf{C}_{\mathrm{M}}^{(1)} &= \frac{1}{V_0} \sum_{i} \sum_{j} (\vec{X}_{(i)}^{\star} \mathbf{K}_{\mathrm{M}}^{(ij)} \vec{X}_{(j)}^{\star})^{LC} \\
{}^{5}\mathbf{C}_{\mathrm{M}}^{(2)} &= \frac{1}{2V_0} \sum_{i} \sum_{j} (\vec{X}_{(i)}^{\star} \mathbf{K}_{\mathrm{M}}^{(ij)} \mathbf{Y}_{(j)}^{\star})^{LC} \\
{}^{5}\mathbf{C}_{\mathrm{M}}^{(3)} &= \frac{1}{2V_0} \sum_{i} \sum_{j} (\mathbf{Y}_{(i)}^{\star} \mathbf{K}_{\mathrm{M}}^{(ij)} \vec{X}_{(j)}^{\star})^{C_{23}} \\
{}^{6}\mathbf{C}_{\mathrm{M}}^{(4)} &= \frac{1}{4V_0} \sum_{i} \sum_{j} (\mathbf{Y}_{(i)}^{\star} \mathbf{K}_{\mathrm{M}}^{(ij)} \mathbf{Y}_{(j)}^{\star})^{C_{23}}
\end{aligned} \tag{105}$$

with the superscript C_{23} indicating conjugation on the second and third indices and

$$\vec{X}_{(i)}^{\star} = \begin{cases} \vec{X}_{(i)} - \vec{X}_{(1)}, & \text{for} \quad i = 1,2,3,4, \\ \int\limits_{\Gamma_{0\mathrm{L}}} (\vec{X}_L - \vec{X}_{(1)}) \, \mathrm{d}\Gamma_0, & \text{for} \quad i = L^{*}, \\ \int\limits_{\Gamma_{0\mathrm{B}}} (\vec{X}_B - \vec{X}_{(1)}) \, \mathrm{d}\Gamma_0, & \text{for} \quad i = B^{*} \end{cases} \tag{106}$$

$$\mathbf{Y}_{(i)}^{\star} = \begin{cases} \vec{X}_{(i)}\vec{X}_{(i)} - \vec{X}_{(1)}\vec{X}_{(1)}, & \text{for} \quad i = 1,2,3,4, \\ \int\limits_{\Gamma_{0\mathrm{L}}} (\vec{X}_L\vec{X}_L - \vec{X}_{(1)}\vec{X}_{(1)}) \, \mathrm{d}\Gamma_0, & \text{for} \quad i = L^{*}, \\ \int\limits_{\Gamma_{0\mathrm{B}}} (\vec{X}_B\vec{X}_B - \vec{X}_{(1)}\vec{X}_{(1)}) \, \mathrm{d}\Gamma_0, & \text{for} \quad i = B^{*} \end{cases} \tag{107}$$

In the second-order computational homogenization framework the macroscopic problem represents a full second gradient continuum (Mindlin, 1964; Toupin, 1964; Fleck and Hutchinson, 1997). For such a second gradient continuum the local equilibrium equation (in the absence of body forces and body moments) is written as

$$\nabla_{0\mathrm{M}} \cdot \left(\mathbf{P}^c_{\mathrm{M}} - (\nabla_{0\mathrm{M}} \cdot {}^3\mathbf{Q}_{\mathrm{M}})^c \right) = \vec{0} \tag{108}$$

The natural boundary conditions associated with this system of partial differential equations are expressed in (i) the surface traction $\vec{t}_{\mathrm{M}}$

$$\begin{aligned} \vec{t}_{\mathrm{M}} &= \vec{N}_{\mathrm{M}} \cdot \left(\mathbf{P}^c_{\mathrm{M}} - (\nabla_{0\mathrm{M}} \cdot {}^3\mathbf{Q}_{\mathrm{M}})^c \right) + (\nabla^s_{0\mathrm{M}} \cdot \vec{N}_{\mathrm{M}}) \vec{N}_{\mathrm{M}} \cdot (\vec{N}_{\mathrm{M}} \cdot {}^3\mathbf{Q}_{\mathrm{M}})^c \\ &- \nabla^s_{0\mathrm{M}} \cdot (\vec{N}_{\mathrm{M}} \cdot {}^3\mathbf{Q}_{\mathrm{M}})^c \end{aligned} \tag{109}$$

where the surface gradient operator is defined as $\nabla^s_{0\mathrm{M}} = (\mathbf{I} - \vec{N}_{\mathrm{M}} \vec{N}_{\mathrm{M}}) \cdot \nabla_{0\mathrm{M}}$ with $\vec{N}_{\mathrm{M}}$ the unit outward normal on the surface of the macroscopic body in the undeformed configuration and (ii) the double stress traction $\vec{r}_{\mathrm{M}}$

$$\vec{r}_{\mathrm{M}} = \vec{N}_{\mathrm{M}} \cdot {}^3\mathbf{Q}_{\mathrm{M}} \cdot \vec{N}_{\mathrm{M}} \tag{110}$$

In the case of a non-smooth surface of the body (with edges) also an additional line load appears. The kinematic boundary conditions for the second gradient continuum include prescribed displacements $\vec{u}_{\mathrm{M}}$ and normal gradients of displacements $D_{0\mathrm{M}} \vec{u}_{\mathrm{M}}$ with $D_{0\mathrm{M}} = \vec{N}_{\mathrm{M}} \cdot \nabla_{0\mathrm{M}}$.

The constitutive equations relating the macroscopic first Piola-Kirchhoff stress tensor $\mathbf{P}_{\mathrm{M}}$ and the higher-order stress tensor ${}^3\mathbf{Q}_{\mathrm{M}}$ to the history of the macroscopic deformation tensor $\mathbf{F}_{\mathrm{M}}$ and its gradient ${}^3\mathbf{G}_{\mathrm{M}}$ are thus obtained numerically, whereas their variations are obtained in the linearized form (102)–(103) with the macroscopic consistent tangents calculated from the condensed microscopic stiffness matrix according to (105).

8.5 Parallel solution of the multi-scale nested boundary value problems

In spite of the large computational effort required by a computational homogenization scheme, it is well possible to make an efficient analysis if optimal use is made of the inherent parallel nature of this multi-scale framework. Whenever microstructural constitutive information is needed in a macroscopic (integration) point, a separate subroutine can be started on the RVE-level that solves the requested boundary value problem. This can be done in parallel in as many integration points as available processors. Using PVM (Parallel Virtual Machine) or MPI (Message Passing Interface), it

is relatively easy to construct such a parallel implementation for this type of problems, as schematically depicted in figure 20. Evidently, this procedure drastically reduces the total calculation time.

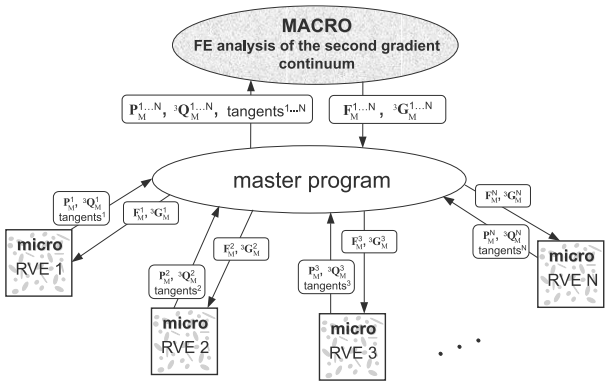

Figure 20. Schematic overview of the parallel solution of the multi-scale nested BVPs

9 Higher-order issues

9.1 First-order versus second-order

The first example concerns the comparison of the mechanical and kinematical response of a heterogeneous microstructure for the first-order and the second-order scale transition. To this purpose, an RVE is considered, which is depicted in its undeformed state in figure 21. The material consid-

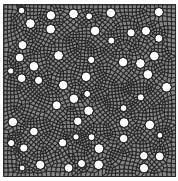

Figure 21. Undeformed two-dimensional RVE of a voided metal

ered is a metal with very weak inclusions, which have a negligible mechanical contribution (e.g. voids). The matrix material is elasto-viscoplastic, constitutively prescribed by a Bodner-Partom viscosity function. Following the

conventional multiplicative split of $\mathbf{F}$, the elastic response is modelled by a classical (isotropic) Neo-Hookean relationship, where the Kirchhoff stress tensor is given by

$$\tau \;=\; K(J-1)\mathbf{I} + G\bar{\mathbf{b}}_e^d \tag{111}$$

In here, J is the volume change ratio, K is the bulk modulus, G is the shear modulus, $\bar{\mathbf{b}}_e^d$ is the deviatoric part of the isochoric elastic left Cauchy-Green deformation tensor. The plastic part is determined through the plastic deformation rate tensor $\mathbf{D}_p$

$$\mathbf{D}_p \;=\; \frac{\sigma^d}{2\eta} \tag{112}$$

where the viscosity η is related to the von Mises equivalent stress σ_e and the effective plastic strain ϵ_p by

$$\begin{aligned} \eta \;&=\; \frac{\sigma_e}{\sqrt{12\Gamma_0}} \exp\left(\frac{1}{2}\left[\frac{Z}{\sigma_e}\right]^{2n}\right) \\ Z \;&=\; Z_1 + (Z_0 - Z_1)\mathrm{e}^{-m\epsilon_p} \end{aligned} \tag{113}$$

with Γ_0, n, Z_0, Z_1 and m material constants. In the present analysis, an aluminum matrix (AA 1050) has been considered for which the material parameters are given by $G = 2.6{\cdot}10^4$ MPa, $K = 7.8{\cdot}10^4$ MPa, $\Gamma_0 = 10^8\,\mathrm{s}^{-2}$, $m = 13.8$, $n = 3.4$, $Z_0 = 81.4$ MPa, $Z_1 = 170$ MPa.

The comparison between the first and second-order formulation is next made for a microstructure with a second phase (12% volume fraction of voids in this case) with an average size of about 6.6 μm. The macroscopic deformation history of a specific material point representing bending with superimposed tension is extracted. This history is imposed to the RVE, after which the micro scale BVP can be solved. The deformed microstructures shown in figure 22 are then obtained for the considered point (with the same macroscopic deformation history!). The deformation modes obtained and the small scale strain fields are obviously different, which reflects the kinematical enrichment of the second-order approximation. Note that the RVE is clearly bending in the second-order case, which is the result of the presence of the higher-order deformation modes that properly account for the size of the microstructure. The periodicity of the microfluctuation field can also be noticed. The macro field however, is no longer periodic for the second-order case.

9.2 Full gradient versus couple stress

Considerable attention has been devoted in the literature to the use of a couple stress theory (Toupin, 1962; Koiter, 1964), in which only the

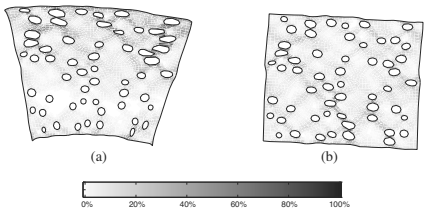

Figure 22. Deformed RVEs for the second-order (a) and first-order (b) RVE with their micro fields of the effective plastic strain

rotational gradient field is taken into account (the curl of $\mathbf{F}_{\mathrm{M}}$). In order to illustrate the contribution of the stretch gradients, the deformation history of a material point in the vicinity of the notch of a notched tensile specimen has been considered. This deformation history is used to construct the full gradient micro scale RVE and the couple stress micro scale RVE, the latter involving the antisymmetric part ${}^{3}\mathbf{G}_{\mathrm{M}}^{A}$ of ${}^{3}\mathbf{G}_{\mathrm{M}}$ only (i.e. switching to index notation, ${}^{3}\mathbf{G}_{\mathrm{M}}^{A} = \frac{2}{3}G_{Mijk} - \frac{1}{3}(G_{Mjki} + G_{Mkij})$, which is a third-order representation of the second-order curvature tensor that is normally used in couple stress theories). The analysis has been performed on the RVE shown in figure 21, with an average void size of $0.13\,\mu$m. The comparison between the full gradient RVE and the couple stress RVE is shown in figure 23. This

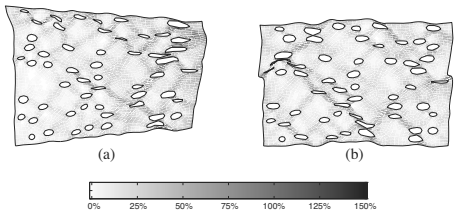

Figure 23. Full gradient, full ${}^{3}\mathbf{G}_{\mathrm{M}}$ (left) deformed RVE versus the couple stress, antisymmetric part of ${}^{3}\mathbf{G}_{\mathrm{M}}$ deformed RVE (right) in the same macroscopic point in the vicinity of the notch of a notched tensile specimen. Equivalent plastic strain fields are depicted inside the RVEs

example illustrates the difference between the full gradient and couple stress case and particularly emphasizes the relevance of the stretch gradients in the scale transition.

9.3 Geometrical size effects

The intrinsic role of the size of the microstructure becomes obvious through the complexity of the deformed RVE obtained and the constitutive response at the microscale which is triggered through the macroscopic deformation. Clearly, large microstructures will show a more pronounced gradient effect (e.g. the bending mode). Performing such a microstructural size analysis in a single macroscopic material point for a given constant loading history but with different underlying microstructures is straightforward. The extracted stress tensors are characteristic for the size effect that has been obtained. The scalar norm of the macroscopic first Piola-Kirchhoff stress tensor $\mathbf{P}_{\mathrm{M}}$ (i.e. defined as $(P_{Mij}P_{Mij})^{1/2}$) and the higher-order tensor ${}^{3}\mathbf{Q}_{\mathrm{M}}$ (i.e. by taking $(Q_{Mijk}Q_{Mijk})^{1/2}$) are good measures to illustrate this, see figure 24. Deviations from the first-order theory are increasingly

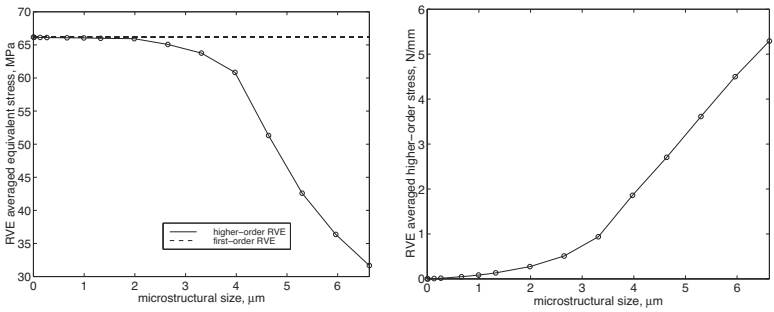

Figure 24. Scalar stress norms of the macroscopic first Piola-Kirchhoff stress tensor (top) and the higher-order stress tensor (bottom) as a function of the microstructural size in a given macroscopic material point

important for larger microstructures. In the limit of an infinitesimal RVE, the first-order solution is always recovered.

9.4 Large macroscopic gradients

For a given microstructure with fixed intrinsic sizes, the second-order framework turns out to be relevant again if local macroscopic deformations tend to be highly non-uniform, i.e. if the gradient ${}^{3}\mathbf{G}_{\mathrm{M}}$ becomes non-negligible with respect to the microstructural size. This is typically the case upon localization of the deformation at the macro scale, where deformations vary strongly in narrow zones. Localization leads to increasing values of ${}^{3}\mathbf{G}_{\mathrm{M}}$, which strongly interacts with the constitutive behaviour of the underlying microstructure. This is shown for the heterogeneous two-phase mate-

rial considered with an average size of the weak phase of 13 μm. The gradient ${}^3\mathbf{G}_{\mathrm{M}}$ is increased proportionally from $G_M^{eq} = ({}^3\mathbf{G}_{\mathrm{M}} \vdots {}^3\mathbf{G}_{\mathrm{M}})^{1/2} = 0\,\mathrm{mm}^{-1}$ to $0.19\,\mathrm{mm}^{-1}$, $0.39\,\mathrm{mm}^{-1}$, $0.78\,\mathrm{mm}^{-1}$ and $0.98\,\mathrm{mm}^{-1}$. The deformed RVEs with their effective plastic strain fields are shown in figure 25. The most left RVE has a zero macroscopic gradient, which reflects a first-order loading mode. For larger gradients, the deformed shape of the RVE becomes clearly more complex (and more representative compared to a first-order result for the real physical geometry of the microstructure).

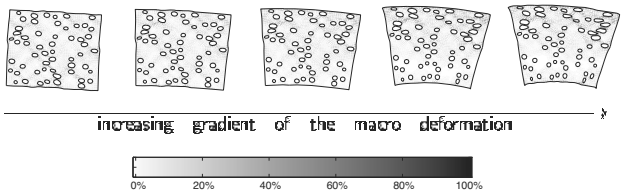

Figure 25. Higher-order RVE response as the result of an increasing macroscopic gradient in a material point with a given microstructure. Equivalent plastic strain fields are depicted inside the RVEs

9.5 Macroscopic localization

In order to scrutinize the added value of the second-order method on the macro scale, an academic benchmark problem was set up in which large macroscopic gradients appear and in which the material softens moderately on the global RVE-scale. The example consists in a periodic micro-voided plate, made of a commercial steel (T67CA), for which the matrix material can be modelled with a (hypo)elasto-perfectly plastic constitutive model ($E = 210$ GPa, $\nu = 0.3$, $\sigma_{y0} = 507$ MPa). The voids in the plate have a diameter of 4 microns, whereas the periodic cell itself measures $d = 10\mu$m, see figure 26. An imperfection (i.e. a reduction) of 20 % is applied to the yield stress in the left bottom cell, in order to trigger the appearance of macroscopic gradients, that may lead to localization of deformations. The second-order equilibrium scheme used requires higher-order boundary conditions that have to be prescribed at the edges of domain. In this case, the bottom and left edge in figure 26 are symmetry axes where normal displacements and tangential stress tractions are taken zero. The top edge undergoes a uniform vertical displacement, whereas the right edge is free. The normal derivatives of the tangential displacement components at the bottom,

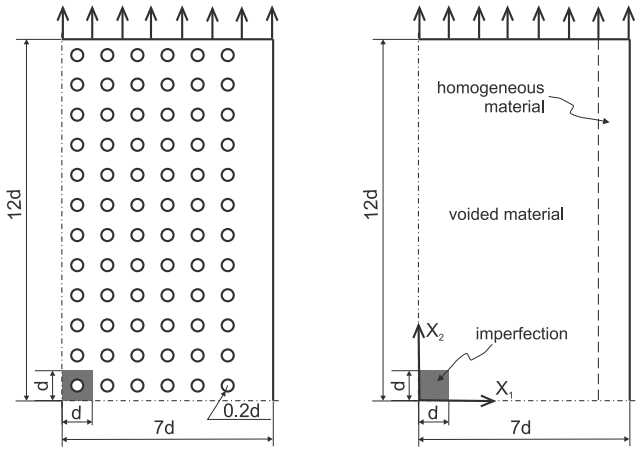

Figure 26. Benchmark problem for computational homogenization analysis

left and top edge are constrained as well. Double stress vectors (Fleck and Hutchinson, 1997) $\vec{N}\cdot{}^{3}\mathbf{Q}_{\mathrm{M}}\cdot\vec{N}$ are zero at all edges.

Strong shear bands occur inside the unit cells, which leads to moderate (geometrical) softening on the global RVE-level, see figure 27. The inade-

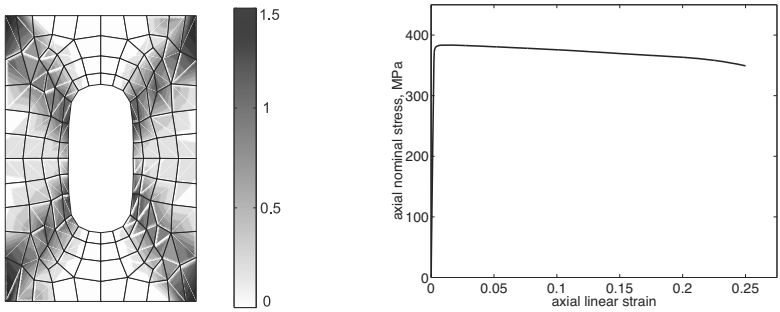

(a) (b)

Figure 27. Single unit cell under uniaxial tension. (a) Deformed geometry and distribution of the equivalent Green-Lagrange strain within the unit cell. (b) Stress-strain response.

quacy of the first-order scheme to deal with this type of behaviour becomes apparent in figure 28, where the prescribed macroscopic displacement measures $0.9\mu m$. In here, the solution for two different mesh sizes is depicted,

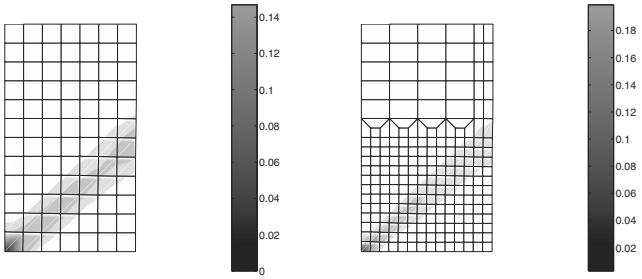

Figure 28. Localized (equivalent) Green-Lagrange strain field for two mesh sizes on the basis of the first-order scheme

where the solution fully localizes according to the size of the elements used. It is not surprising, that this homogenization method suffers from exactly the same shortcomings as classical (local) constitutive softening models as extensively investigated by many authors in the past decade (Schreyer and Chen, 1986; Bažant and Pijaudier-Cabot, 1988; Aifantis, 1992; de Borst and Mühlhaus, 1992; de Borst and Pamin, 1996; Peerlings et al., 1996; Svedberg and Runesson, 1997; Geers et al., 1998; Engelen et al., 2003). This property is inherently linked to the principle of local action, which associates for each macroscopic point a volume with infinitesimal size at the RVE level. Upon further refinement of the macroscopic mesh, the energy dissipated in the softening RVE on the micro-scale is in fact dissipated in a shrinking volume at the macroscopic scale, which is one of the main manifestations of the ill-posedness of the boundary value problem (at the macro scale) to be solved.

The second-order computational homogenization method leads to a higher-order boundary value problem, for which the regularizing effects are known to exist. The size of the microstructural volume element implicitly sets the length scale in the macro scale analysis, which makes the numerical solution independent of the mesh size (the localization band converges to a finite width), see figure 29.

A two-scale overview of the deformed state of the perforated plate is shown in figure 30. Note that the behaviour ensuing from a regularized continuum theory for failure at the micro scale or a well-posed discrete failure model at the micro scale cannot be upscaled with a first-order homogenization method. In fact, the well-posedness at the micro scale basically implies that the corresponding constitutive response at the macro scale does not depend on the discretization at the micro scale. This is of course a necessary condition, though not sufficient. The volume in which the energy was

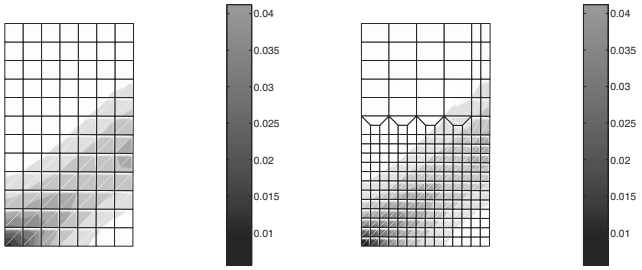

Figure 29. Localized (equivalent) Green-Lagrange strain field for two mesh sizes on the basis of the second-order scheme

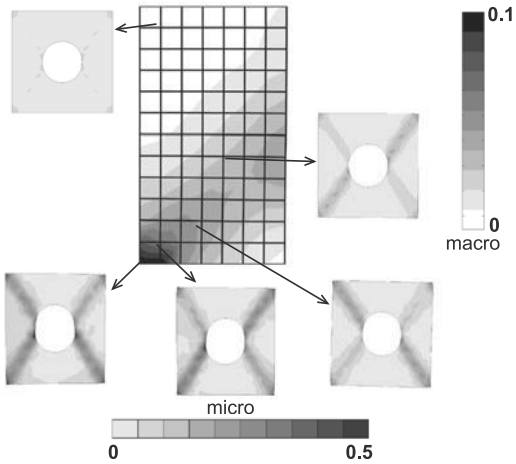

Figure 30. Deformed unit cell patterns and their equivalent Green-Lagrange strain fields embedded in the corresponding macroscopic solution field

dissipated at the micro scale has to be transported correctly to the macro scale to prevent loss of well-posedness at the macro scale. This is impossible within the standard local continuum mechanics framework (first-order scheme), which again underlines the need for higher-order homogenization methods for the upscaling of failure processes accompanied by macroscopic softening.

9.6 The higher-order RVE

It has already been emphasized that the requirement of statistical representativeness constituted an important aspect in the definition of an RVE for a classical first-order homogenization approach. As a result, there was no restriction on the (maximum) size of a representative cell (on the contrary, taking the first-order RVE as large as possible, allows to represent given statistical characteristics more accurately). This is related to the fact that the first-order computational homogenization scheme (as well as most other conventional homogenization methods) deals with an ordinary local continuum on the macroscopic level. Such a continuum does not possess a material length scale and accordingly the size of a microstructural cell does not play a role. For the second-order case, size does play a role and the definition of an RVE is therefore not trivial. A detailed analysis on this subject has been performed in Kouznetsova et al. (2004b). In here, it has been shown that the size of the microstructural RVE used in a second-order computational homogenization scheme is intrinsically related to the length scale of the resulting macroscopic homogenized higher-order continuum. Furthermore, material and geometrical non-linearities significantly contribute to the relation between the RVE size and the obtained macroscopic response. In a second-order computational homogenization two conflicting requirements on the microstructural representative volume element have to be accommodated. On the one hand, the accurate determination of the overall behaviour of a multi-phase material requires a large representative cell with many (interacting) heterogeneities. On the other hand, the size of a representative cell used in the second-order computational homogenization scheme implicitly sets the length scale of the macroscopic homogenized higher-order continuum.

In most cases, it is possible to give a reasonable estimate of the required size of the representative cell based on the qualitative assessment of the basic mechanisms of the underlying microstructural evolution, interaction and the statistics of the considered microstructure. The lower limit for the size of the RVE should be selected as the minimum size that contains enough microstructural features to allow the development of the governing microstructural physical mechanisms that are relevant for the problem under consideration. The upper limit for the RVE size directly results from the underlying assumption that the macroscopic deformations vary linearly over the microstructural cell. If this assumption does not apply (i.e. if the macroscopic deformations vary too strongly on the scale of the microstructural constituents) a computational homogenization scheme can never provide accurate results, since a separation of scales is not applicable. In such cases the analysis should be performed by detailed microstructural mod-

elling. This, in fact, sets an upper limit on the RVE size, which may be used for the second-order homogenization analysis.

10 Conclusions

This contribution presented an overview of two computational homogenization techniques for the multi-scale analysis of the mechanical behaviour of (physically and geometrically) complex microstructures. It has been shown that length scales can be bridged more accurately by transferring more information between the two scales considered. Rigourous scale transitions have been established by making use of averaging theorems and the Hill-Mandel energy condition. The first-order computational homogenization strategy fully complies with the principle of local action and the principle of separation of scales. The kinematics are essentially based on the linearization of the macroscopic nonlinear deformation map. The second-order case was based on the proper incorporation of the macroscopic gradient of the deformation tensor into the kinematical micro-macro framework. Work-conjugated stress and higher-order stress tensors are naturally retrieved and a full gradient continuum is obtained on the macro scale. The main advantage of the performed scale transition resides in the fact that the constitutive response (either first- or second-order) is obtained directly from the collective behaviour of all constituent phases at the micro scale. No assumptions need to be made on the format of the macroscopic constitutive relationship, which makes the proposed scale transition a versatile tool to assess macroscopic constitutive relations. Furthermore, the methodology can be fully implemented in a hierarchical solution scheme, where two nested boundary value problems have to be solved. Consistency of the tangent operator is preserved by the scale transition. The presented two-scale framework is parallel in its nature, which makes the implementation of the numerical solution method on a multi-processor cluster clearly beneficial.

Whether or not a second-order model should be used has to be decided considering the governing scales, loading and the presence of failure/softening. Whenever the principle of separation of scales continues to hold, macroscopic gradients remain small and failure does not occur, it is certainly recommended to use the first-order computational homogenization method. However, if damage and failure are of interest and need to be linked to microstructural events, it is obvious that a higher-order technique will be necessary. Even if a well-posed regularized solution strategy (either continuum or discrete) is used on the micro level, a second-order scheme will remain necessary. The length scale, which may be well defined on the microstructural scale is not preserved through a first-order scale transition.

Evidently, this becomes most apparent for failure analyses with softening.

Likewise, geometrical size effects, for which the size of the microstructure is not negligible with respect to the geometry of the macro-specimen, have to be captured by such a technique as well. Note that microstructural size effects, which emerge from size-dependent small scale deformation mechanisms (e.g. dislocation plasticity leading to the Hall-Petch effect, the Friedel effect, etc.) can still be upscaled appropriately with a first-order scheme. In here, the microstructural size effect becomes apparent in the constitutive response of the microstructural phases. Most important property of a second-order method is the fact that it implicitly incorporates a length scale, which depends on the size of the microstructure. This size becomes apparent on the macro-scale as the length scale that sets the width of localization zones, or that governs geometrical size effects. The role of the RVE size in a second-order scheme is crucial and has been discussed extensively in Kouznetsova et al. (2004b).

Computational homogenization seems to make constitutive modelling considerably easier. The first-order or second-order constitutive response (which is difficult to capture in a closed format with its constitutive tensors), is retrieved directly from the microstructure. This is particularly useful to assess the homogenized 'continuum' response of microstructural discrete systems, in which e.g. atomistics, molecular dynamics or discrete dislocation dynamics are used to obtain the fine scale response. Undoubtedly, many issues are still to be explored: assessing higher-order boundary conditions from the microstructure, upscaling various failure mechanisms within the microstructure that lead to macroscopic degradation, the appearance of geometrical size effects in miniaturization, etc.

Bibliography

E. C. Aifantis. On the role of gradients in the localization of deformation and fracture. *International Journal of Engineering Science*, 30:1279–1299, 1992.

F. P. T. Baaijens. Calculation of residual stresses in injection-molded products. *Rheol. Acta*, 30:284–299, 1991.

M. W. Barsoum, P. Kangutkar, and A. S. D. Wang. Matrix crack initiation in ceramic matrix composites. Part I: Experiments and test results. *Composites Science and Technology*, 44:257–269, 1992.

Z. P. Bažant and G. Pijaudier-Cabot. Nonlocal continuum damage, localization instability and convergence. *Journal of Applied Mechanics*, 55: 287–293, 1988.

J. R. Brockenbrough, S. Suresh, and H. A. Wienecke. Deformation of metal-

matrix composites with continuous fibers: geometrical effect of fiber distribution and shape. *Acta Metall. Mater.*, 39(5):735–752, 1991.

P. W. Chung, K. K. Tamma, and R. R. Namburu. Asymptotic expansion homogenization for heterogeneous media: computational issues and applications. *Composites Part A: Applied Science and Manufacturing*, 32 (9):1291–1301, 2001.

R. D. Cook, D. S. Malkus, and M. E. Plesha. *Concepts and applications of finite element analysis*. Wiley, Chichester, 1989.

R. de Borst and H. B. Mühlhaus. Gradient-dependent plasticity: Formulation and algorithmic aspects. *International Journal for Numerical Methods in Engineering*, 35:521–539, 1992.

R. de Borst and J. Pamin. Some novel developments in finite elemet procedures for gradient-dependent plasticity and finite elements. *International Journal for Numerical Methods in Engineering*, 39:2477–2505, 1996.

W. J. Drugan and J. R. Willis. A micromechanics-based nonlocal constitutive equation and estimates of representative volume element size for elastic composites. *Journal of the Mechanics and Physics of Solids*, 44 (4):497–524, 1996.

R. A. B. Engelen, M. G. D. Geers, and F. P. T. Baaijens. Nonlocal implicit gradient-enhanced softening plasticity. *International Journal of Plasticity*, 2003. In press.

F. Feyel and J. L. Chaboche. FE^2 multiscale approach for modelling the elasto-viscoplastic behaviour of long fibre SiC/Ti composite materials. *Computer Methods in Applied Mechanics and Engineering.*, 183:309–330, 2000.

J. Fish and W. Chen. Higher-order homogenization of initial/boundary-value problem. *Journal of Engineering Mechanics*, 127(12):1223–1230, 2001.

J. Fish, Kamlun Shek, Muralidharan Pandheeradi, and Mark S. Shephard. Computational plasticity for composite structures based on mathematical homogenization: Theory and practice. *Computer Methods in Applied Mechanics and Engineering*, 148(1-2):53–73, 1997.

N. A. Fleck and J. W. Hutchinson. Strain gradient plasticity. *Advances in Applied Mechanics*, 33:295–361, 1997.

S. Forest, F. Pradel, and K. Sab. Asymptotic analysis of heterogeneous Cosserat media. *International Journal of Solids and Structures*, 38:4585–4608, 2001.

K. Garikipati and T. J. R. Hughes. A variational multiscale approach to strain localization - formulation for multidimensional problems. *Computer Methods in Applied Mechanics and Engineering*, 188(1-3):39–60, 2000.

M. G. D. Geers, R. de Borst, W. A. M. Brekelmans, and R. H. J. Peerlings. Strain-based transient-gradient damage model for failure analyses. *Computer Methods in Applied Mechanics and Engineering*, 160(1-2):133–154, 1998.

M. G. D. Geers, V. G. Kouznetsova, and W. A. M. Brekelmans. Gradient-enhanced computational homogenization for the micro-macro scale transition. *Journal de Physique IV*, 11(5):5145–5152, 2001.

M.G.D. Geers, V.G. Kouznetsova, and W.A.M. Brekelmans. Multi-scale second-order computational homogenization of microstructures towards continua. *International Journal for Multiscale Computational Engineering*, 1(4):371–386, 2003.

S. Ghosh, K. Lee, and S. Moorthy. Multiple scale analysis of heterogeneous elastic structures using homogenisation theory and Voronoi cell finite element method. *International Journal of Solids and Structures*, 32(1): 27–62, 1995.

S. Ghosh, K. Lee, and S. Moorthy. Two scale analysis of heterogeneous elastic-plastic materials with asymptotic homogenization and Voronoi cell finite element model. *Computer Methods in Applied Mechanics and Engineering*, 132:63–116, 1996.

S. Ghosh, K. Lee, and P. Raghavan. A multi-level computational model for multi-scale damage analysis in composite and porous materials. *International Journal of Solids and Structures*, 38(14):2335–2385, 2001.

L. E. Govaert, P. H. M. Timmermans, and W. A. M. Brekelmans. The influence of intrinsic strain softening on strain localization in polycarbonate: modeling and experimental validation. *J. Engrg. Mat. Technol.*, 122:177–185, 2000.

J. M. Guedes and N. Kikuchi. Preprocessing and postprocessing for materials based on the homogenization method with adaptive finite element methods. *Computer Methods in Applied Mechanics and Engineering*, 83: 143–198, 1990.

R. A. Hall. Computer modelling of rubber-toughened plastics: random placement of monosized core-shell particles in a polymer matrix and interparticle distance calculations. *J. Mater. Sci.*, 26:5631–5636, 1991.

R. Hill. Elastic properties of reinforced solids: some theoretical principles. *JJournal of the Mechanics and Physics of Solids*, 11:357–372, 1963.

R. Hill. On macroscopic effects of heterogeneity in elastoplastic media at finite strain. *Math. Proc. Camb. Phil. Soc.*, 95:481–494, 1984.

C. Huet. Application of variational concepts to size effects in elastic heterogeneous bodies. *J. Mech. Phys. Solids*, 38(6):813–841, 1990.

C. Huet. Coupled size and boundary-condition effects in viscoelastic heterogeneous and composite bodies. *Mechanics of Materials*, 31:787–829, 1999.

T. J. R. Hughes, G. R. Feijóo, L. Mazzei, and J. Quincy. The variational multiscale method - a paradigm for computational mechanics. *Computer Methods in Applied Mechanics and Engineering*, 166:3–24, 1998.

W. T. Koiter. Couple-stresses in the theory of elasticity. In *Proceedings of the Koninklijke Nederlandse Akademie van Wetenschappen. Series B*, volume 67, pages 17–44, 1964.

V. G. Kouznetsova. *Computational homogenization for the multi-scale analysis of multi-phase materials.* PhD thesis, Eindhoven University of Technology, Mechanical Engineering Department, December 2002.

V. G. Kouznetsova, W. A. M. Brekelmans, and F. P. T. Baaijens. An approach to micro-macro modeling of heterogeneous materials. *Computational Mechanics*, 27:37–48, 2001.

V. G. Kouznetsova, M. G. D. Geers, and W. A. M. Brekelmans. Advanced constitutive modeling of heterogeneous materials with a gradient-enhanced computational homogenization scheme. *International Journal for Numerical Methods in Engineering*, 54:1235–1260, 2002.

V.G. Kouznetsova, M.G.D. Geers, and W.A.M. Brekelmans. Multi-scale second-order computational homogenization of multi-phase materials: a nested finite element solution strategy. *Computer Methods in Applied Mechanics and Engineering*, 193:5525–5550, 2004a.

V.G. Kouznetsova, M.G.D. Geers, and W.A.M. Brekelmans. Size of a representative volume element in a second-order computational homogenization framework. *International Journal for Multiscale Computational Engineering*, 2(4):575–598, 2004b.

I. Jasiuk M. Ostoja-Starzewski, S. D. Boccara. Couple-stress moduli and characteristic length of a two-phase composite. *Mechanics Research Communications*, 26(4):387–396, 1999.

R. A. Mackay. Effect of fiber spacing on interfacial damage in a metal matrix composite. *Scripta Metall. Mater.*, 24:167–172, 1990.

J. C. Michel, H. Moulinec, and P. Suquet. Effective properties of composite materials with periodic microstructure: a computational approach. *Computer Methods in Applied Mechanics and Engineering*, 172:109–143, 1999.

C. Miehe. Numerical computation of algorithmic (consistent) tangent moduli in large-strain computational inelasticity. *Comput. Methods Appl. Mech. Engrg.*, 134:223–240, 1996.

C. Miehe. Strain-driven homogenization of inelastic microstructures and composites based on an incremental variational formulation. *International Journal for Numerical Methods in Engineering*, 55:1285–1322, 2002.

C. Miehe. Computational micro-to-macro transitions for discretized microstructures of heterogeneous materials at finite strains based on the minimization of averaged incremental energy. *Computer Methods in Applied Mechanics and Engineering*, 192:559–591, 2003.

C. Miehe and A. Koch. Computational micro-to-macro transition of discretized microstructures undergoing small strain. *Archives in Applied Mechanics*, 72:300–317, 2002.

C. Miehe, J. Schotte, and M. Lambrecht. Homogenization of inelastic solid materials at finite strains based on incremental minimization principles. application to the texture analysis of polycrystals. *Journal of the Mechanics and Physics of Solids*, 50(10):2123–2167, 2002.

C. Miehe, J. Schotte, and J. Schröder. Computational micro-macro transitions and overall moduli in the analysis of polycrystals at large strains. *Computational Materials Science*, 16(1-4):372–382, 1999a.

C. Miehe, J. Schröder, and J. Schotte. Computational homogenization analysis in finite plasticity. Simulation of texture development in polycrystalline materials. *Computer Methods in Applied Mechanics and Engineering*, 171:387–418, 1999b.

R. D. Mindlin. Microstructure in linear elasticity. *Arch. Ration. Mech. Anal.*, 16:51–78, 1964.

N. Moës and T. Belytschko. Extended finite element method for cohesive crack growth. *Engineering Fracture Mechanics*, 69(7):813–833, 2002.

H. Moulinec and P. Suquet. A numerical method for computing the overall response of non-linear composites with complex microstructure. *Computer Methods in Applied Mechanics and Engineering*, 157:69–94, 1998.

T. Nakamura and S. Suresh. Effect of thermal residual stress and fiber packing on deformation of metal-matrix composites. *Acta Metall. Mater.*, 41(6):1665–1681, 1993.

S. Nemat-Nasser. Averaging theorems in finite deformation plasticity. *Mechanics of Materials*, 31:493–523, 1999.

S. Nemat-Nasser and M. Hori. *Micromechanics: overall properties of heterogeneous materials*. Elsevier, Amsterdam, 1993.

O. Nguyen and M. Ortiz. Coarse-graining and renormalization of atomistic binding relations and universal macroscopic cohesive behavior. *Journal of the Mechanics and Physics of Solids*, 2002. In Press, Available online.

M. Ostoja-Starzewski. Random field models of heterogeneous materials. *Int. J. Solids Structures*, 35(19):2429–2455, 1998.

M. Ostoja-Starzewski. Scale effects in materials with random distributions of needles and cracks. *Mechanics of Materials*, 31:883–893, 1999.

S. Pecullan, L. V. Gibiansky, and S. Torquato. Scale effects on the elastic behavior of periodic and hierarchical two-dimentional composites. *J. Mech. Phys. Solids*, 47:1509–1542, 1999.

R. H. J. Peerlings, R. de Borst, W. A. M. Brekelmans, and J. H. P. de Vree. Gradient-enhanced damage for quasi-brittle materials. *International Journal for Numerical Methods in Engineering*, 39:3391–3403, 1996.

R. H. J. Peerlings and N. A. Fleck. Numerical analysis of strain gradient effects in periodic media. *Journal de Physique IV*, 11:153–160, 2001.

P. Ponte Castañeda. New variational principles in plasticity and their application to composite materials. *Journal of the Mechanics and Physics of Solids*, 40:1757–1788, 1992.

P. Ponte Castañeda. Second-order homogenization estimates for nonlinear composites incorporating field fluctuations: I theory. *Journal of the Mechanics and Physics of Solids*, 50(4):737–757, 2002.

K. Ridderbos. The coarse-graining approach to statistical mechanics: how blissful is our ignorance? *Studies In History and Philosophy of Science Part B: Studies In History and Philosophy of Modern Physics*, 33(1): 65–67, 2002.

H. L. Schreyer and Z. Chen. One-dimensional softening with localization. *Journal of Applied Mechanics*, 53:791–979, 1986.

Z. Shan and A. M. Gokhale. Representative volume element for non-uniform micro-structure. *Comp. Mat. Sci.*, 24:361–379, 2002.

R. J. M. Smit. *Toughness of heterogeneous polymeric systems*. PhD thesis, Eindhoven University of Technology, Eindhoven, The Netherlands, 1998.

R. J. M. Smit, W. A. M. Brekelmans, and H. E. H. Meijer. Prediction of the mechanical behaviour of non-linear systems by multi-level finite element modeling. *Computer Methods in Applied Mechanics and Engineering*, 155:181–192, 1998.

R. J. M. Smit, W. A. M. Brekelmans, and H. E. H. Meijer. Prediction of the large-strain mechanical response of heterogeneous polymer systems: local and global deformation behaviour of a representative volume element of voided polycarbonate. *J. Mech. Phys. Solids*, 47:201–221, 1999.

V. P. Smyshlyaev and K. D. Cherednichenko. On rigorous derivation of strain gradient effects in the overall behaviour of periodic heterogeneous media. *Journal of the Mechanics and Physics of Solids*, 48:1325–1357, 2000.

V. P. Smyshlyaev and N. A. Fleck. Bounds and estimates for linear composites with strain gradient effects. *Journal of the Mechanics and Physics of Solids*, 42(12):1851–1882, 1994.

N. Sukumar, N. Moës, Moran, and T. Belytschko. Extended finite element method for three-dimensional crack modelling. *International Journal for Numerical Methods in Engineering*, 48(11):1549–1570, 2000.

P. M. Suquet. *Plasticity today: modelling, methods and applications*, chapter Local and global aspects in the mathematical theory of plasticity, pages 279–310. Elsevier Applied Science Publishers, London, 1985.

P. M. Suquet. Overall potentials and extremal surfaces of power law or ideally plastic composites. *Journal of the Mechanics and Physics of Solids*, 41:981–1002, 1993.

T. Svedberg and K. Runesson. A thermodynamically consistent theory of gradient-regularized plasticity coupled to damage. *International Journal of Plasticity*, 13(6-7):669–696, 1997.

K. Terada, M. Hori, T. Kyoya, and N. Kikuchi. Simulation of the multi-scale convergence in computational homogenization approaches. *International Journal of Solids and Structures*, 37(16):2285–2311, 2000.

K. Terada and N. Kikuchi. Nonlinear homogenization method for practical applications. In S. Ghosh and M. Ostaja-Starzewski, editors, *Computational Methods in Micromechanics*, volume AMD-Vol.212, MD-Vol.62, pages 1–16. ASME, 1995.

K. Terada and N. Kikuchi. A class of general algorithms for multi-scale analyses of heterogeneous media. *Computer Methods in Applied Mechanics and Engineering*, 190(40-41):5247–5464, 2001.

T. Tervoort. *Constitutive modelling of polymer glasses: finite, nonlinear viscoelastic behaviour of polycarbonate*. PhD thesis, Eindhoven University of Technology, Eindhoven, The Netherlands, 1996.

R. A. Toupin. Elastic materials with couple-stress. *Archive for Rational Mechanics and Analysis*, 11:385–414, 1962.

R. A. Toupin. Theories of elasticity with couple-stress. *Arch. Ration. Mech. Anal.*, 17:85–112, 1964.

N. Triantafyllidis and S. Bardenhagen. The influence of scale size on the stability of periodic solids and the role of associated higher order gradient continuum models. *Journal of the Mechanics and Physics of Solids*, 44 (11):1891–1928, 1996.

H. C. E. van der Aa, M. A. H. van der Aa, P. J. G. Schreurs, F. P. T. Baaijens, and W. J. van Veenen. An experimental and numerical study of the wall ironing process of polymer coated sheet metal. *Mechanics of Materials*, 32:423–443, 2000.

O. van der Sluis, P. J. G. Schreurs, W. A. M. Brekelmans, and H. E. H. Meijer. Overall behaviour of heterogeneous elastoviscoplastic materials: effect of microstructural modelling. *Mechanics of Materials*, 32:449–462, 2000.

O. van der Sluis, P. H. J. Vosbeek, P. J. G. Schreurs, and H. E. H. Meijer. Homogenization of heterogeneous polymers. *International Journal of Solids and Structures*, 36:3193–3214, 1999.